Sex-dependent compensatory mechanisms preserve blood pressure homeostasis in prostacyclin receptor deficient mice

[1]Soon Yew Tang, PhD; [1]Hu Meng, PhD, [1]Seán T. Anderson, PhD; [1]Dimitra Sarantopoulou, MSc; [1]Soumita Ghosh, PhD; [1]Nicholas F. Lahens, PhD; [1]Katherine N. Theken, [1]Emanuela Ricciotti, PhD; [1]Elizabeth J. Hennessy, PhD; [2]Vincent Tu, PhD; [2]Kyle Bittinger, PhD; [1]Aalim Weiljie, PhD; [1,3]Gregory R. Grant, PhD; [1]*Garret A. FitzGerald, MD

[1]From the Institute for Translational Medicine and Therapeutics, Department of Systems Pharmacology and Translational Therapeutics, Perelman School of Medicine, University of Pennsylvania, Philadelphia, Pennsylvania, USA., [2]Division of Gastroenterology, Hepatology, and Nutrition, Children's Hospital of Philadelphia, Philadelphia, Pennsylvania, USA. [3]Department of Genetics, University of Pennsylvania, Philadelphia, Pennsylvania, USA.

[1]*Garret A. FitzGerald, MD

[1]From the Institute for Translational Medicine and Therapeutics, Perelman School of Medicine, Department of Systems Pharmacology and Translational Therapeutics, [2]Department of Genetics, University of Pennsylvania, Philadelphia, Pennsylvania, 19104-5127. [3]Current address at National Institute on Aging, National Institutes of Health, 21224.

*Address for correspondence: Garret A. FitzGerald, Institute for Translational Medicine and Therapeutics, Perelman School of Medicine, 10-110 Smilow Center for Translational Research, 3400 Civic Center Blvd, Bldg 421, University of Pennsylvania, Philadelphia, PA 19104-5158. Fax: 215-573-9135 Tel: 215-898-1184 Email: garret@upenn.edu

Subject code: Vascular Disease

Supplemental Table 1. Differentially expressed genes identified in eIF2 signaling, mitochondrial dysfunction and oxidative phosphorylation pathways in kidney medulla in male mice.

eIF2						OP & MD				MD	
Gene	**Log_2FC**	**Gene**	**Log_2FC**	**Gene**	**Log_2FC**	**Gene**	**Log_2FC**	**Gene**	**Log_2FC**	**Gene**	**Log_2FC**
Acta2	0.432	Rpl14	-0.664	Rpl7a	-0.333	Atp5e	-0.991	Ndufa4	-0.884	Aco1	0.259
Ago2	0.438	Rpl15	-0.404	Rps3	-0.666	Atp5c1	-0.26	Ndufa5	-0.41	Aco2	0.293
Cdk11b	-0.196	Rpl17	-1.033	Rps6	-0.702	Atp5g3	-0.342	Ndufa6	-0.448	App	0.491
Eif2s3x	0.459	Rpl19	-0.515	Rps7	-0.699	Atp5j2	-0.601	Ndufa12	-0.361	Cat	0.423
Eif3e	-0.316	Rpl21	-0.495	Rps8	-0.651	Atp5l	-0.693	Ndufab1-ps	-0.374	Gpd2	0.403
Eif3h	-0.406	Rpl22	-0.765	Rps11	-0.795	Atp5j	-0.541	Ndufb1-ps	-0.994	Gpx4	-0.452
Eif3m	-0.359	Rpl23	-0.384	Rps12	-1.08	Atp5o	-0.417	Ndufb2	-0.752	Lrrk2	0.491
Eif4g1	0.469	Rpl24	-0.784	Rps13	-0.861	Cox15	0.484	Ndufb3	-0.381	Mapk12	-0.578
Eif4g2	0.32	Rpl26	-0.861	Rps14	-0.682	Cox17	-0.519	Ndufb4c	-0.915	mt-Nd6	-0.711
Eif4g3	0.314	Rpl27	-0.59	Rps16	-0.66	Cox5a	-0.261	Ndufb5	-0.481	Ncstn	0.278
Grb2	0.224	Rpl30	-0.771	Rps17	-0.83	Cox6c2	-0.646	Ndufb6	-0.641	Ogdh	0.268
Map2k1	0.356	Rpl31	-0.908	Rps18	-0.647	Cox6c	-0.688	Ndufb8	-0.509	Psen1	0.238
Mapk1	0.367	Rpl32l	-1.083	Rps19	-0.932	Cox7a1	-0.708	Ndufb9	-0.665	Sod2	0.185
Pdpk1	0.547	Rpl35	-0.802	Rps20	-0.724	Cox7a2	-0.836	Ndufb10	-0.388		
Pik3c2a	0.626	Rpl37	-0.769	Rps21	-0.934	Cox7a2l	-0.4	Ndufb11	-0.428		
Pik3cb	0.38	Rpl38	-0.844	Rps23	-0.845	Cox7b	-0.824	Ndufs1	0.323		
Pik3r4	0.326	Rpl39	-0.929	Rps24	-1.19	mt-Atp6	-0.726	Ndufs4	-0.729		
Rpl3	-0.448	Rpl41	-0.775	Rps25	-1.007	mt-Co1	-0.508	Ndufs6b	-0.742		
Rpl5	-0.804	Rpl10a	-0.538	Rps28	-0.541	mt-Co2	-0.994	Ndufv2	-0.37		
Rpl6l	-0.531	Rpl13a	-0.723	Rps15a	-0.946	mt-Co3	-0.985	Uqcrb	-0.446		
Rpl7	-0.373	Rpl22l1	-1.157	Rps27a	-1.091	mt-Cytb	-0.589	Uqcrh-ps1	-0.557		
Rpl9	-0.966	Rpl27a	-0.803	Rps27l	-1.056	mt-Nd1	-0.548				
Rpl10	-0.433	Rpl35a	-0.95	Rps4x	-0.572	mt-Nd3	-0.864				
Rpl11	-0.622	Rpl36a	-0.6	Rpsa	-0.61	mt-Nd4	-0.606				
Rpl12	-0.876	Rpl36al	-0.463			Ndufa1	-0.498				
Rpl13	-0.486	Rpl37a	-0.724			Ndufa3	-0.652				

eIF2, eukaryotic initiation factor, MD, mitochondrial dysfunction, OP, oxidative phosphorylation

Supplemental Table 2. Functional output analysis predicted inflammatory responses in atria of female mice.

Diseases/ Function	*P*-value/ Q-value	Activation z-score	Molecules
Chronic inflammatory disorder	4.41E-07/ 1.47E-03	NA	Add2, Apoe, C5ar1, Casp1, Cd53, Cdkal1, Ckm, Cyp2b10, Gbp6, Gipr, H2-Q2, H2-DMb1, H2-Aa, H2-M3, Hs3st3b1, Ifi213, Mpeg1, Mtr, Nlrc5, Pglyrp1, Pptc7, Prkcq, Psmb9, Ptprc, Sele, Sting1, Tlr1, Tnfrsf10b, Trim28
Activation of leukocytes	6.06E-06/ 2.76E-03	-0.932	Apoe, Bloc1s3, C5ar1, Casp1, Ceacam1, H2-Q2, H2-DMb1, H2-Aa, H2-M3, Lair1, Gm15931, Milr1, Nectin2, Prkcq, Psmb9, Ptprc, Sele, Sting1, Tlr1, Tnfrsf10b
Cell-mediated response	3.33E-04/ 3.95E-02	-1.021	Apoe, C5ar1, Casp1, H2-Q2, H2-M3, Nectin2, Sting1, Vasp

Supplemental Figures

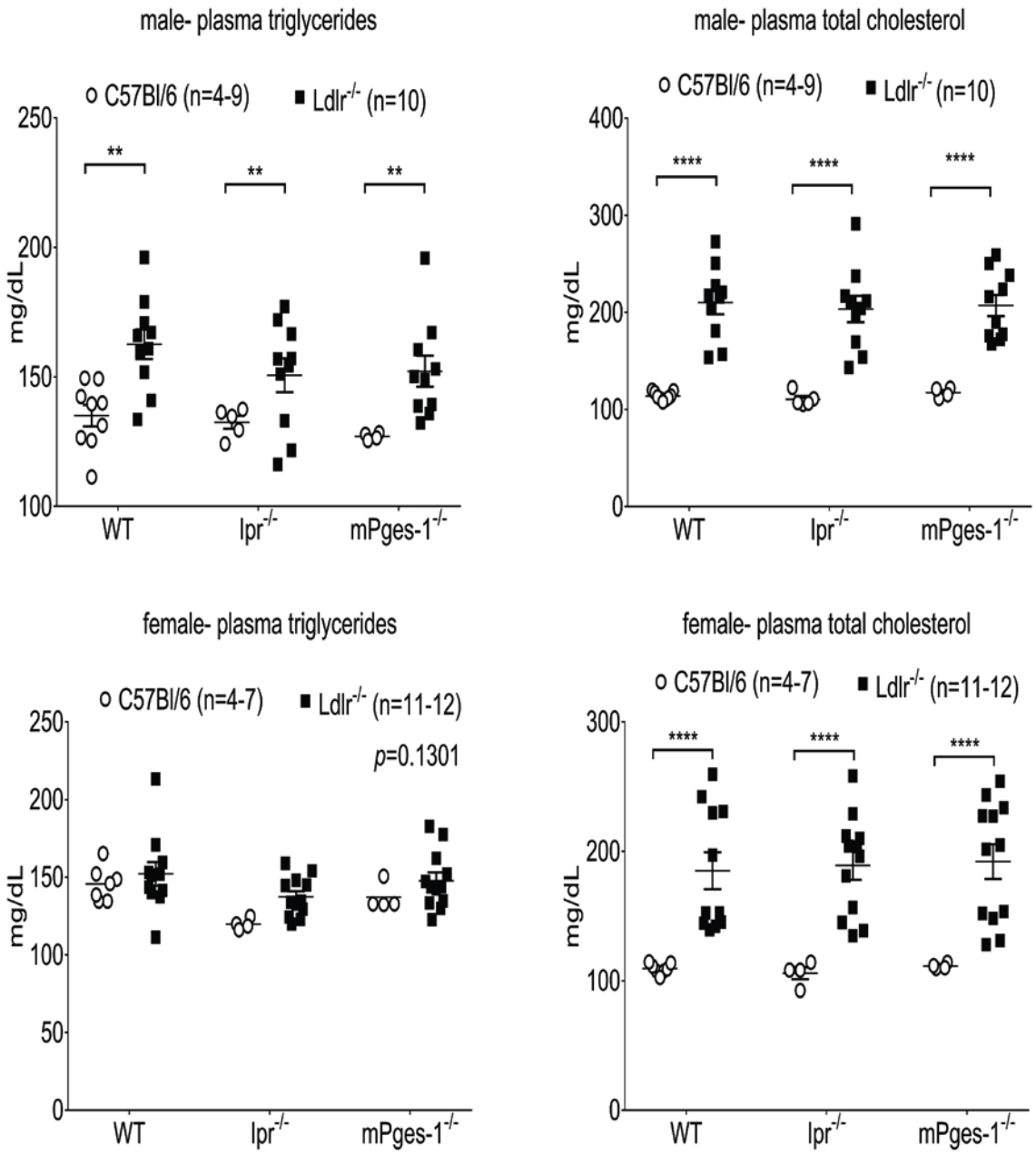

Supplemental Figure 1. Low density lipoprotein receptor (Ldlr)-deficient mice were hyperlipidemia. Ipr- and mPges-1-deficient mice of both sexes on C57Bl/6 and $Ldlr^{-/-}$ genetic backgrounds between eight to ten weeks old on chow diet were sacrificed for blood collection. Plasma samples were separated and used for measurement of triglyceride and total cholesterol

levels following manufacturer's instructions. A parametric t-test (2 tailed) revealed a significant effect of $Ldlr^{-/-}$ on plasma triglycerides (A) and total cholesterol (B) levels in male wild-type (WT), Ipr- and mPges-1-deficient mice. In female mice, plasma total cholesterol levels (D) were significantly elevated in mice on the $Ldlr^{-/-}$ background but not plasma triglyceride levels (C). Data are expressed as means ± SEMs. $^{**}p<0.01$, $^{****}p<0.0001$; n= 4-12 per group.

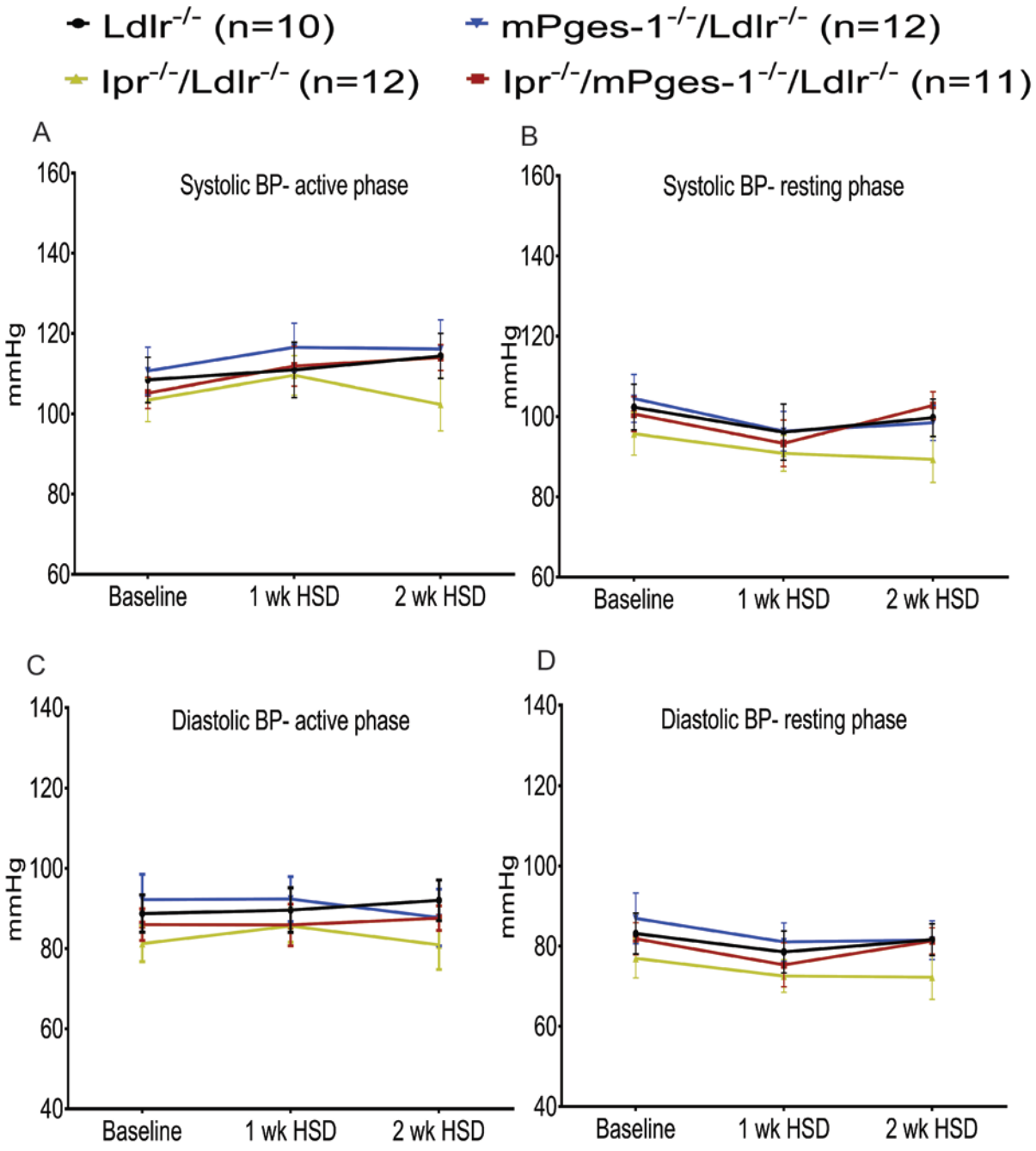

Supplemental Figure 2. Salt loading did not alter blood pressures in female hyperlipidemic mice. Systolic blood pressures (SBP) in female hyperlipidemic mice and Ipr-, mPges-1- and Ipr/mPges-1-deficient mutants on Ldlr$^{-/-}$ background fed a high salt diet (HSD) were measured via telemetry. HSD did not significantly alter SBP (A and B) and DBP (C and D) in the mutants

and their littermate controls ($Ldlr^{-/-}$), during the active phase (A and C, night) and resting phase (B and D, day). 4-way ANOVA with repeated measures and Greenhouse-Geisser correction showed no significant effects of Ipr ($p > 0.05$), treatment ($p > 0.05$), mPges-1 ($p > 0.05$) and week ($p > 0.05$) on salt-evoked elevation in SBP and DBP, although phase ($p = 0$) is significantly affecting both SBP and DBP. Data are expressed as means ± SEMs. n=10-12 per genotype.

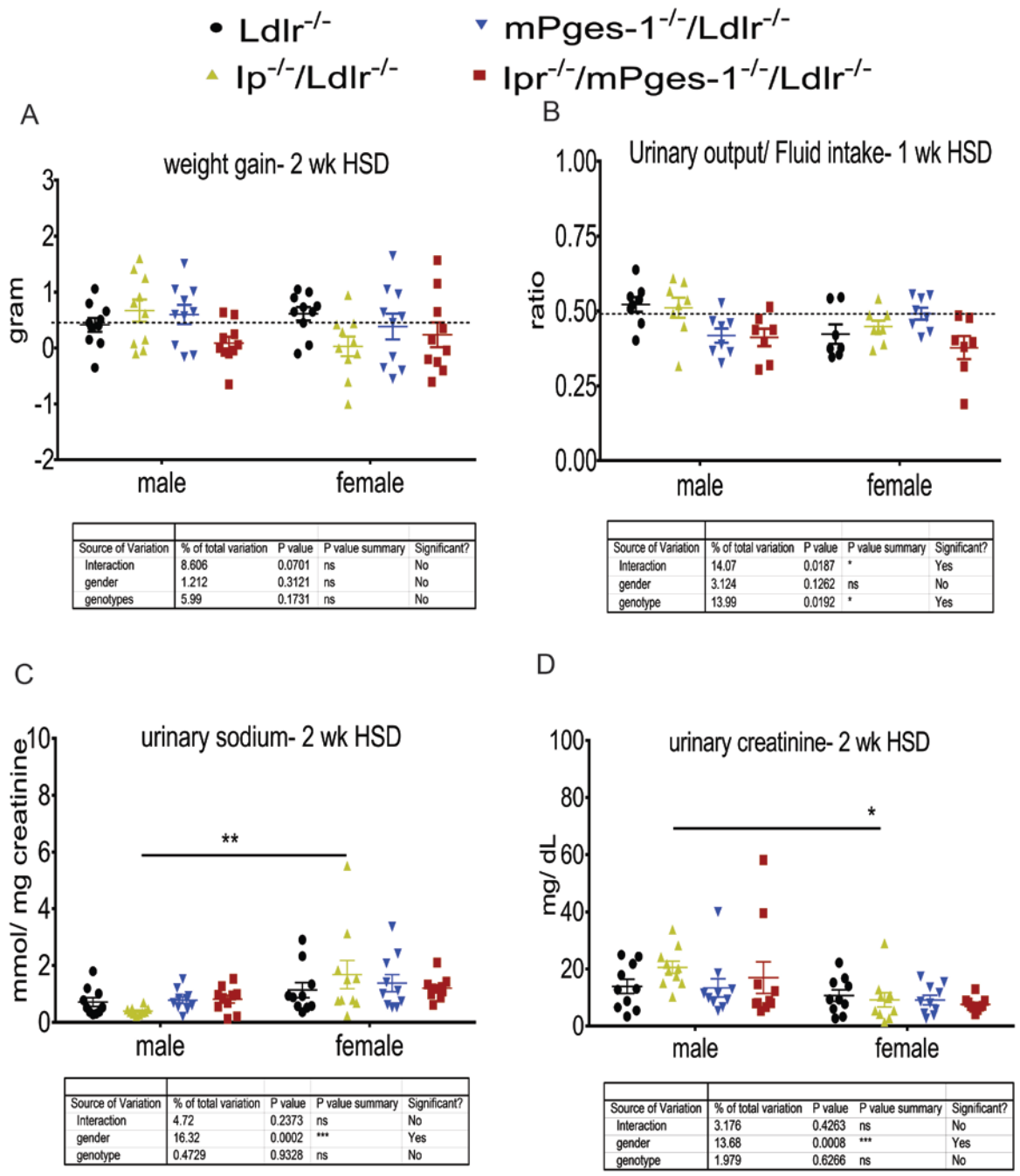

Source of Variation	% of total variation	P value	P value summary	Significant?
Interaction	8.606	0.0701	ns	No
gender	1.212	0.3121	ns	No
genotypes	5.99	0.1731	ns	No

Source of Variation	% of total variation	P value	P value summary	Significant?
Interaction	14.07	0.0187	*	Yes
gender	3.124	0.1262	ns	No
genotype	13.99	0.0192	*	Yes

Source of Variation	% of total variation	P value	P value summary	Significant?
Interaction	4.72	0.2373	ns	No
gender	16.32	0.0002	***	Yes
genotype	0.4729	0.9328	ns	No

Source of Variation	% of total variation	P value	P value summary	Significant?
Interaction	3.176	0.4263	ns	No
gender	13.68	0.0008	***	Yes
genotype	1.979	0.6266	ns	No

Supplemental Figure 3. Weight gain, urinary output/ fluid ratio, urinary sodium and creatinine levels between male and female mice. Mice were weighed before and after feeding an HSD for 2 weeks. Urinary output and fluid intake was performed at week 1 during the HSD to ensure consistency in harvesting tissues, urine and blood at the end of week 2. Urinary sodium

levels were measured following manufacturer's instructions. Urinary creatinine was measured using LC-MS as described in the Methods. Two-way ANOVA revealed no significant effect of gender on weight gain (A) and urinary output/ fluid intake ratio (B). Urinary sodium (C) and creatinine levels (D) of female Ipr$^{-/-}$/Ldlr$^{-/-}$ mice was significantly higher and lower than male Ipr$^{-/-}$/Ldlr$^{-/-}$ mice, respectively. Multiple comparison tests (Holm-Sidak) were used to test significant differences of weight gain between male and female mice. Data are expressed as means ± SEMs. *p<0.05, **p<0.01; n=7-10 per genotype.

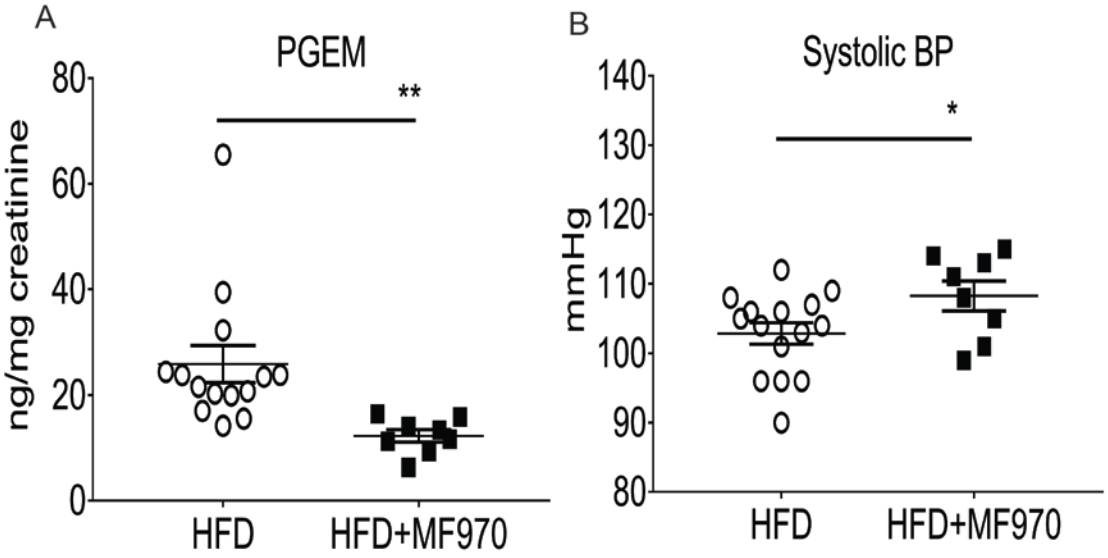

Supplemental Figure 4. Pharmacological inhibition of mPGES-1 enzyme suppresses PGE_2 biosynthesis and elevates systolic blood pressure. Eight weeks old male humanized mPges-1 hyperlipidemic mice were put on a high fat diet (HFD) alone or in conjunction with an inhibitor specific for human mPGES-1 enzyme (MF970) for 39 weeks. At the end of the HFD, blood

pressure was measured using a tail-cuff system and urine samples were collected for prostanoid metabolites measurement by LC/ MS as detailed in the Methods. MF970 administration suppressed urinary PGE_2 metabolite (A) and elevated SBP (B). Data are expressed as means ± SEMs (Parametric test, one-tailed, *p< 0.05, **p< 0.01). n=8-15 per group. We used a one-tailed test for urinary PGEM and systolic BP because MF970 has been shown to suppress PGE_2 biosynthesis and PGE_2 regulates BP homeostasis.

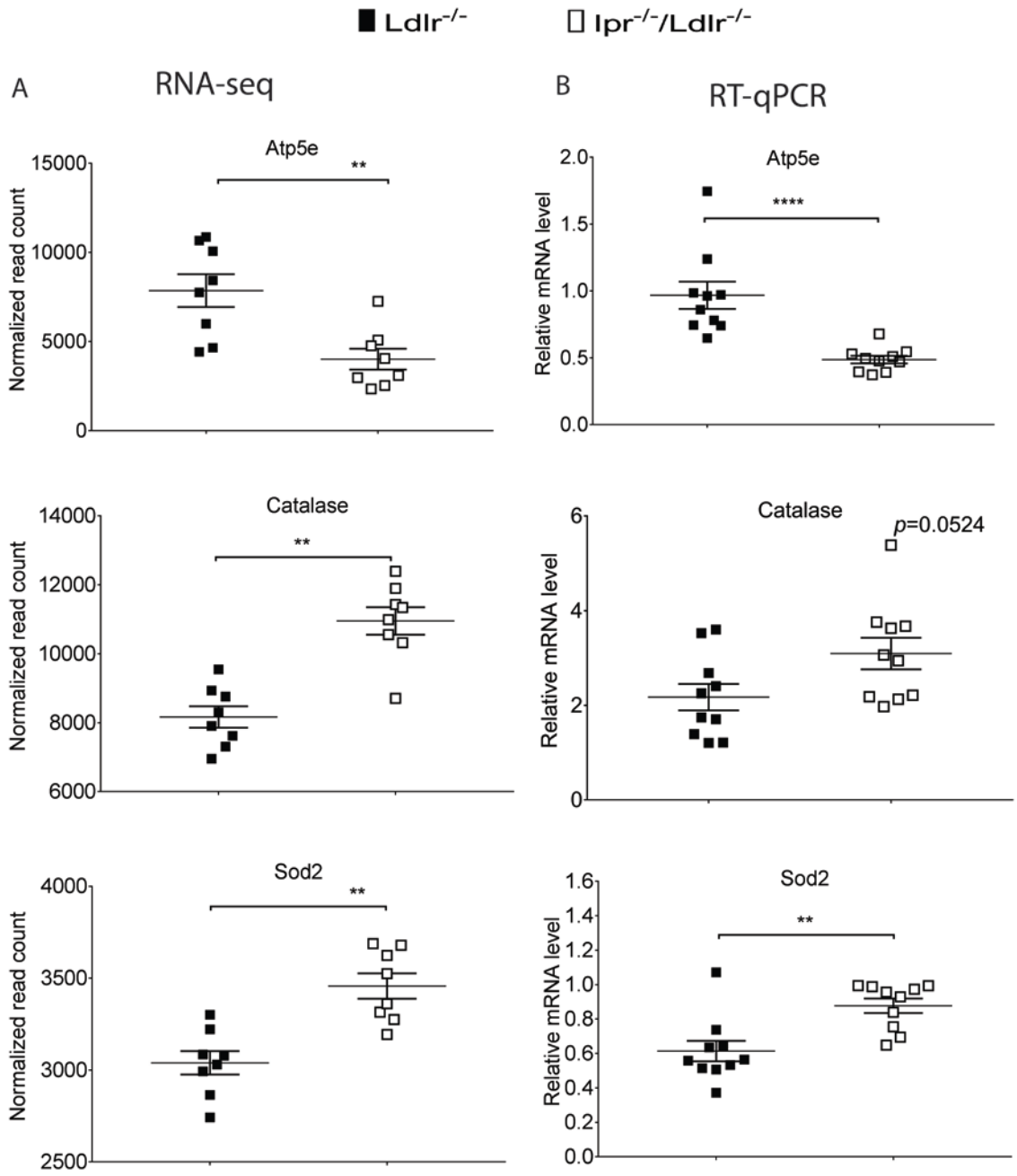

Supplemental Figure 5. Validation of RNA-Seq transcripts in kidney medulla of male mice by RT-qPCR. RNA samples isolated from kidney medulla of Ldlr$^{-/-}$ and Ipr$^{-/-}$/Ldlr$^{-/-}$ after two weeks on an HSD were used for real-time PCR analyses. RNA-seq transcripts of three genes (A-Atp5e, catalase and Sod2) in mitochondrial dysfunction and oxidative phosphorylation pathways were consistent with their mRNA levels as detected by RT-qPCR (B). Data are expressed as

means ± SEMs (Parametric test, two-tailed, **p<0.01, ***p<0.001, ****p<0.0001). n=8 per genotype for RNA-seq, n=10 per genotype for RT-qPCR.

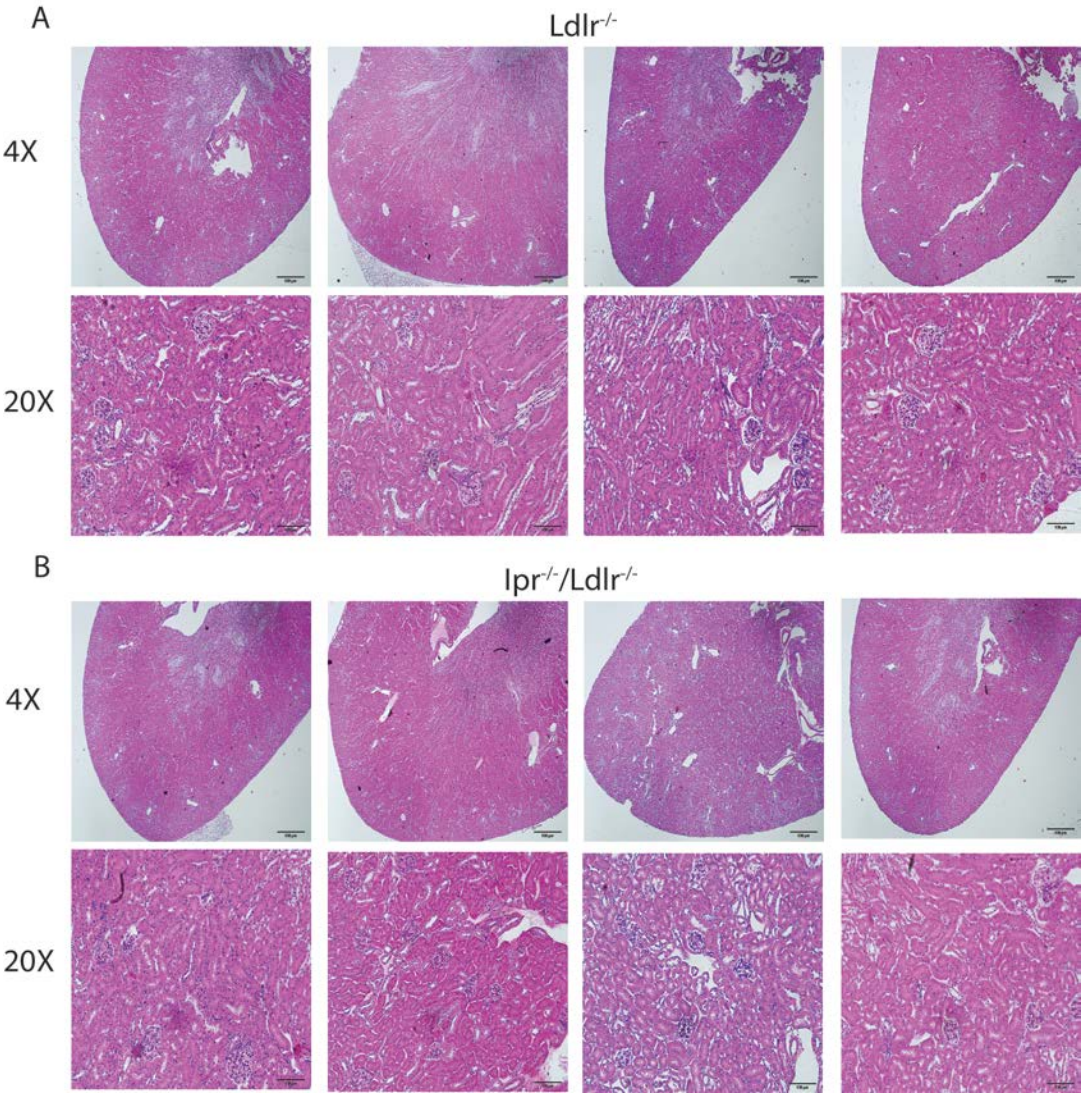

Supplemental Figure 6. Morphological characteristics of kidney of male Ldlr$^{-/-}$ and Ipr$^{-/-}$ /Ldlr$^{-/-}$ mice fed a high salt diet for two weeks.

After feeding an HSD for 2 weeks, kidneys of male Ldlr$^{-/-}$ (A) and Ipr$^{-/-}$/Ldlr$^{-/-}$ (B) mice were formalin fixed and paraffin embedded. Five µm serial sections (6-8 sections) of the tissues were cut and mounted on Superfrost Plus slides for analysis of tissue morphology by HE staining. n= 4 per genotype.

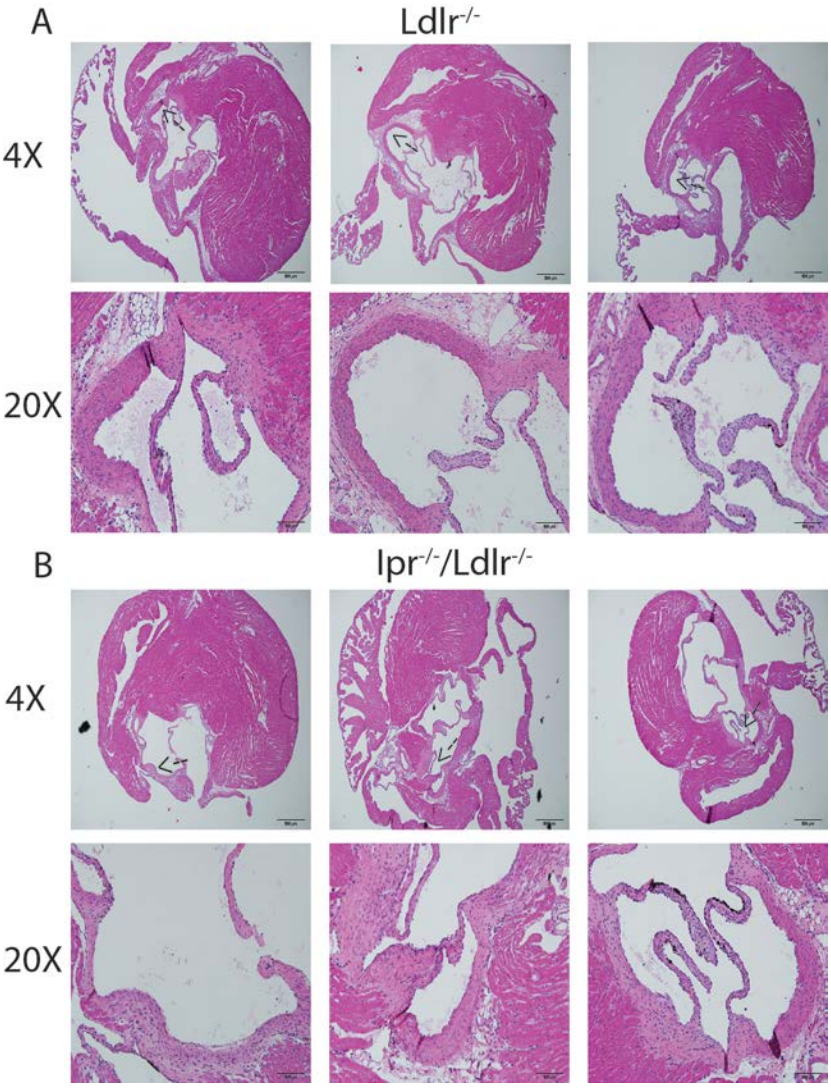

Supplemental Figure 7. Morphological characteristics of vasculature of male Ldlr$^{-/-}$ and Ipr$^{-/-}$/Ldlr$^{-/-}$ mice fed a high salt diet for two weeks.

After feeding an HSD for 2 weeks, aortic roots of male Ldlr$^{-/-}$ (A) and Ipr$^{-/-}$/Ldlr$^{-/-}$ (B) mice were formalin fixed and paraffin embedded. Five µm serial sections (8-10 sections) of the tissues were cut and mounted on Superfrost Plus slides for analysis of tissue morphology by HE staining. n= 3 per genotype. → indicates area of 20X magnification.

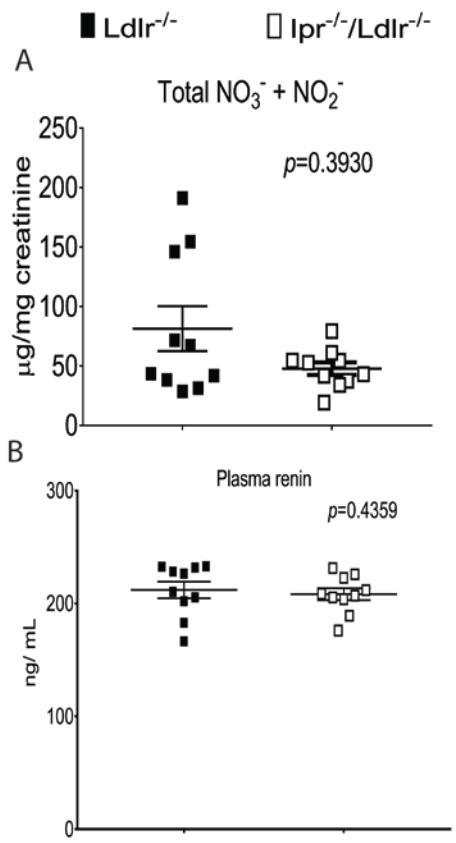

Supplemental Figure 8. Impact of Ipr deletion on urinary total nitrate+ nitrite and sodium and plasma renin levels in male hyperlipidemic mice on a high salt diet. Fasting (9am-4pm) urine samples from $Ldlr^{-/-}$ and $Ipr^{-/-}/Ldlr^{-/-}$ mice were collected two weeks after feeding an HSD. Deletion of Ipr in $Ldlr^{-/-}$ mice did not significantly alter urinary total nitrate+ nitrite (A) and plasma renin (B). Data are expressed as means ± SEMs (Parametric test, two-tailed, $p > 0.05$, n=10 per genotype).

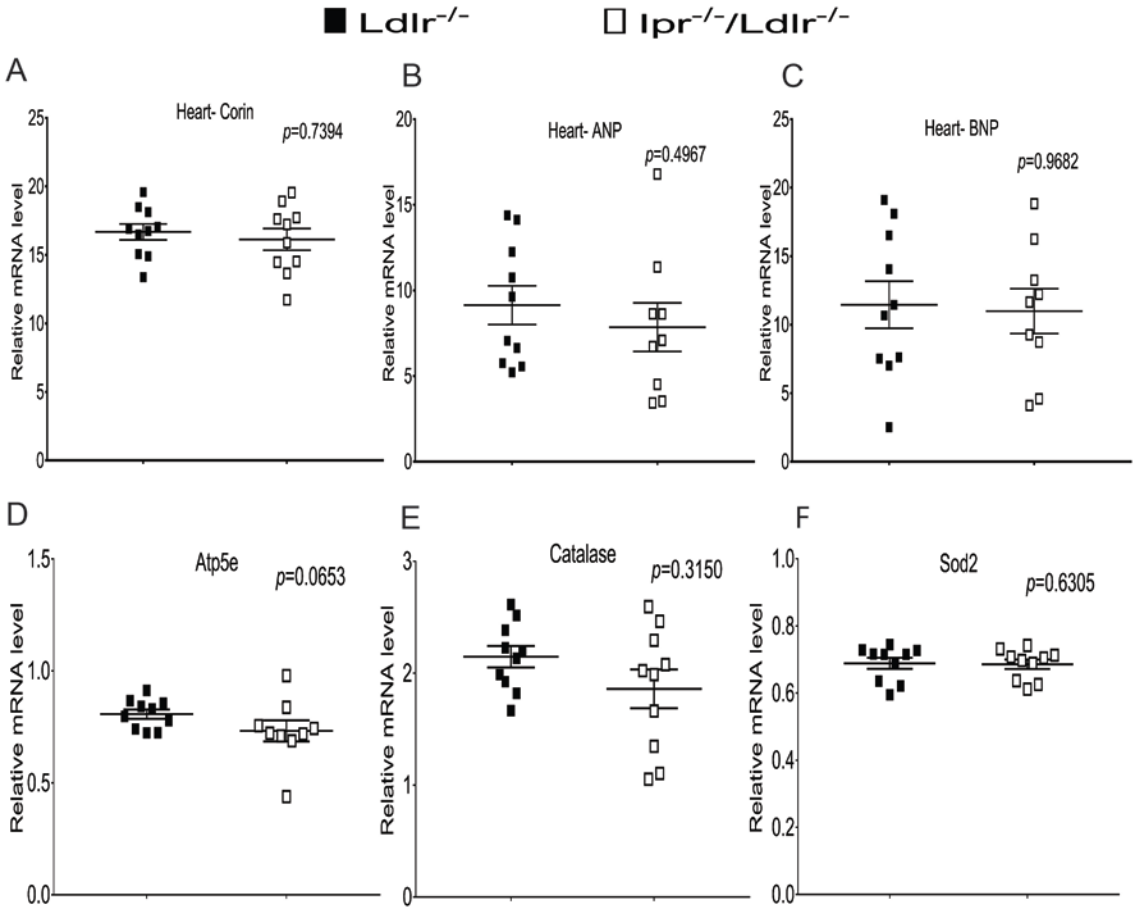

Supplemental Figure 9. Deletion of Ipr did not alter mRNA expression of corin, atrial natriuretic peptide and brain natriuretic peptide in heart and ATP5e, catalase and superoxide dismutase 2 in kidney medulla of female mice fed a high salt diet. RNA samples isolated from whole heart and kidney medulla of $Ldlr^{-/-}$ and $Ipr^{-/-}/Ldlr^{-/-}$ mice after two weeks on an HSD were used for real-time PCR analyses. No significant differences in corin (A- ANP converting enzyme), atrial natriuretic peptide (B- heart ANP), brain natriuretic peptide (C- heart BNP) and kidney medullary Atp5e (D), Cat (E) and Sod2 (F) were observed between $Ldlr^{-/-}$ and $Ipr^{-/-}/Ldlr^{-/-}$ mice. Data are expressed as means ± SEMs (Parametric test, two-tailed, $p > 0.05$; n=9-10 per genotype).

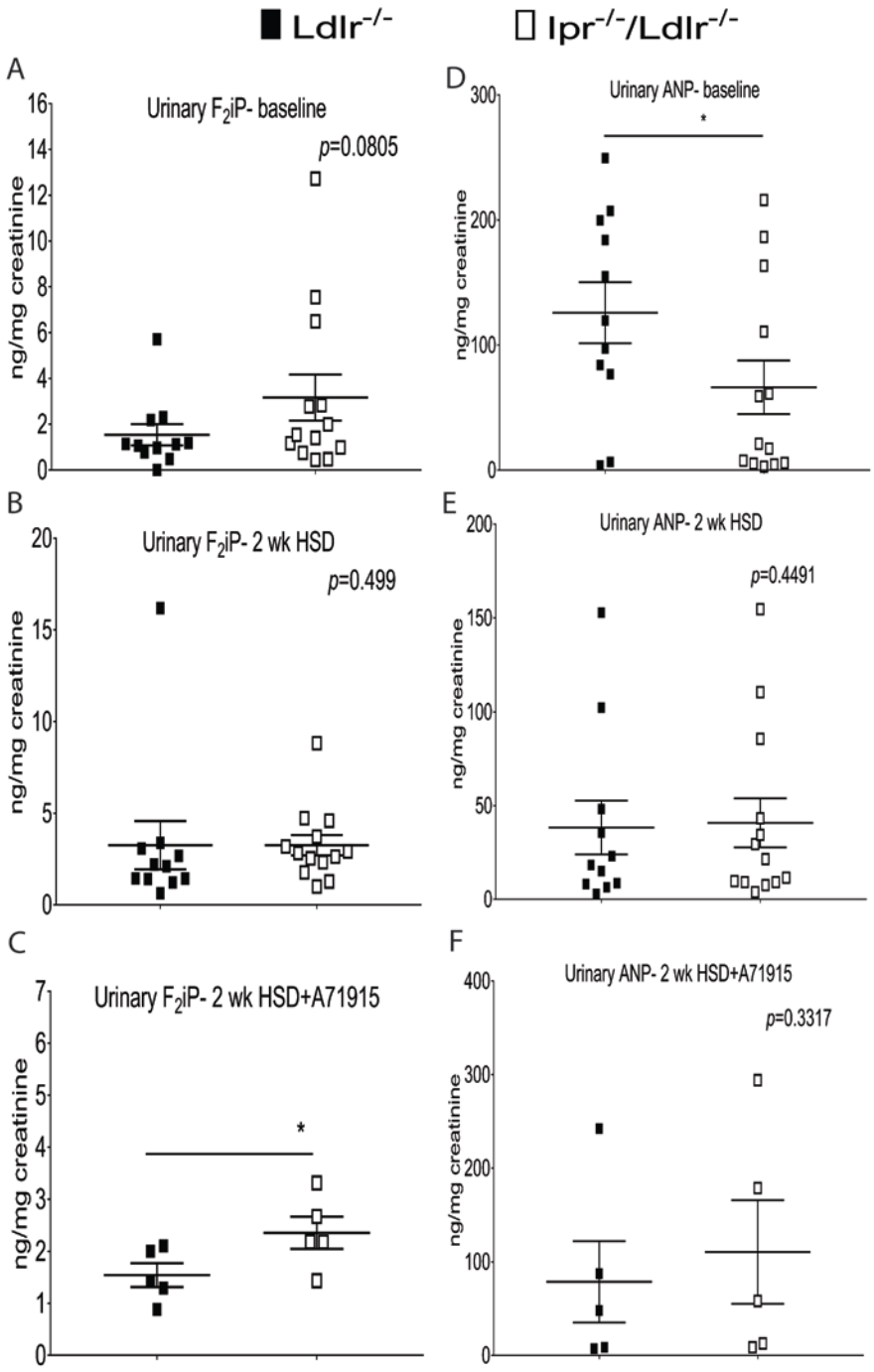

Supplemental Figure 10. The effect of combined deletion of Ipr and salt-evoked hypertension on urinary F_2-isoprostane and atrial natriuretic peptide in female mice.

Urinary F_2-isoprostane (F_2iP) was analyzed by liquid chromatography/ mass spectrometry as described in the methods. (A) Deletion of $Ipr^{-/-}$ in $Ldlr^{-/-}$ mice did not significantly increase

baseline (A) and two weeks (B) after an HSD compared with $Ldlr^{-/-}$ mice (n=11-13). Deletion of Ipr and blockade of ANP receptor with A71915 (50 µg/Kg BW/ day) significantly increase urinary F_2iP after feeding an HSD (C, n=5). Urinary ANP was measured using an ELISA kit following manufacturer's instructions. (D) Deletion of Ipr in $Ldlr^{-/-}$ mice significantly decrease baseline urinary ANP compared with $Ldlr^{-/-}$ mice (n=11-13). This difference was abolished two weeks after feeding the mice an HSD alone (E) and in conjunction with the ANP receptor antagonist, A71915 (F, n=5). Data are expressed as means ± SEMs (Parametric test, Welch's correction, one-tailed, $*p < 0.05$). We used a one-tailed test for urinary F_2iP and ANP because both mediators have been shown to restrain oxidative stress in the vasculature.

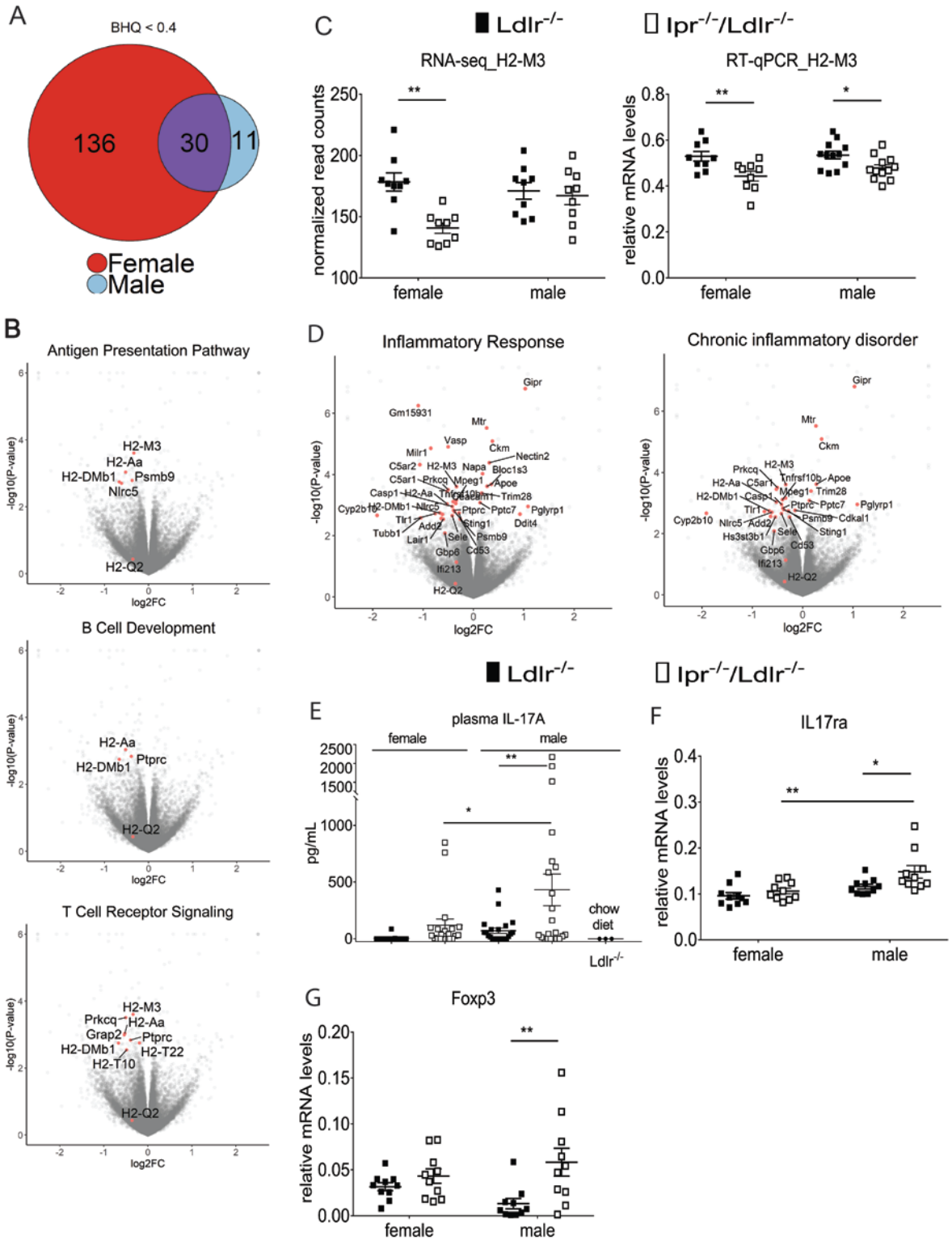

Supplemental Figure 11. Sex-dependent immunological responses induced by a HSD. RNA samples isolated from atria of Ldlr$^{-/-}$ and Ipr$^{-/-}$/Ldlr$^{-/-}$ after two weeks on a HSD were used for

RNA-Seq. (A) Venn diagram of DEGs between female and male mice. 136 genes were unique to female, 11 genes were unique to male and 30 genes were common between female and male. (B) Analysis of signaling pathways. Volcano plots compare genes identified in the top three canonical pathways: antigen presentation, B cell development and T cell receptor signaling. (C) H2-M3 gene was validated by RT-qPCR (n= 9-13). (D) Volcano plots of DEGs-predicted downstream functional output as inflammatory responses and chronic inflammatory disorder. (E) Plasma IL-17A was measured using an ELISA kit following manufacturer's instruction. Deletion of Ipr increased HSD-induced plasma levels of IL-17A in male $Ldlr^{-/-}$ mice. (F-G) Real-time PCR was used to measure the expression of cardiac IL-17ra (IL-17 receptor A) and Foxp3 (transcription factor of T-regulatory cells). HSD increased IL-17ra and Foxp3 transcripts in the heart of male $Ipr^{-/-}/Ldlr^{-/-}$ mice compared with $Ldlr^{-/-}$ mice. Two-way ANOVA showed a significant effect of sex or genotype on plasma levels of IL-17A, IL-17ra and Foxp3. Sidak's multiple comparison tests were used to test significant differences between sexes or genotypes. Data are expressed as means ± SEMs, $*p< 0.05$, $**p< 0.01$, plasma IL-17A, n= 20-22 per genotype, male $Ldlr^{-/-}$ on chow diet, n= 3; IL-17ra and Foxp3, n= 10 per genotype.

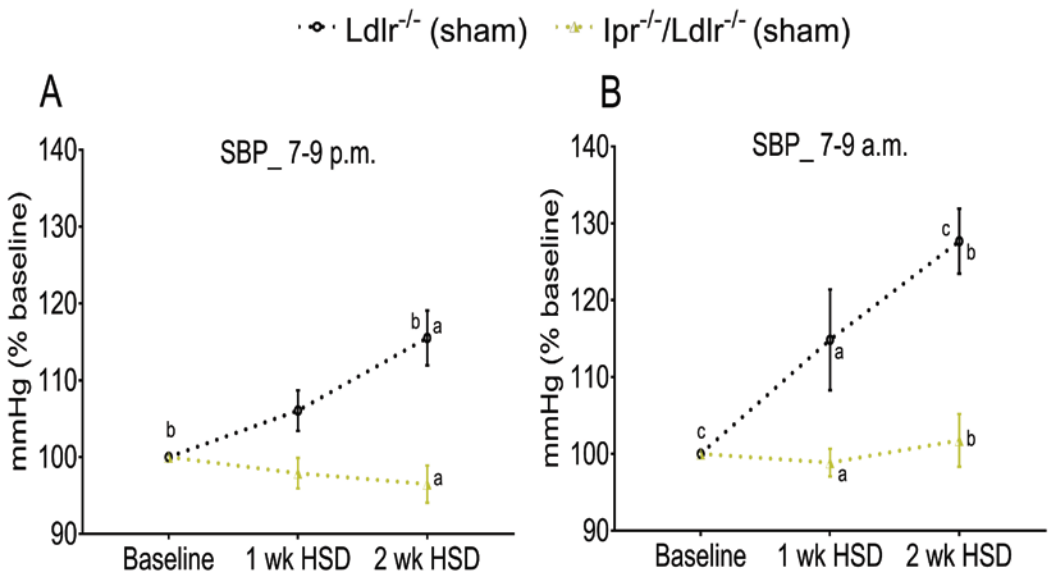

Supplemental Figure 12. Saline infused via mini-pumps did not rescue hypotension in Ipr-deficient male hyperlipidemic mice fed a high salt diet. Systolic blood pressures (SBP, A- night, B- day) of male mice with mini-pumps containing saline were measured using a tail-cuff system before, one and two weeks after feeding an HSD. Two-way ANOVA revealed a significant effect of genotype and/ or feeding time on SBP responses during the active phase (genotype, $p< 0.05$, feeding time, $p< 0.0001$, interaction, $p< 0.001$) and resting phase (genotype, $p< 0.01$, feeding time, $p< 0.0001$, interaction, $p< 0.01$). Multiple comparison tests (Holm-Sidak) were used to test significant differences between $Ldlr^{-/-}$ and $Ipr^{-/-}/Ldlr^{-/-}$ mice and among different feeding times. Genotype and/ or feeding time with the same lower case letter are significantly different (a- c). Data are expressed as means ± SEMs. n=6 per genotype.

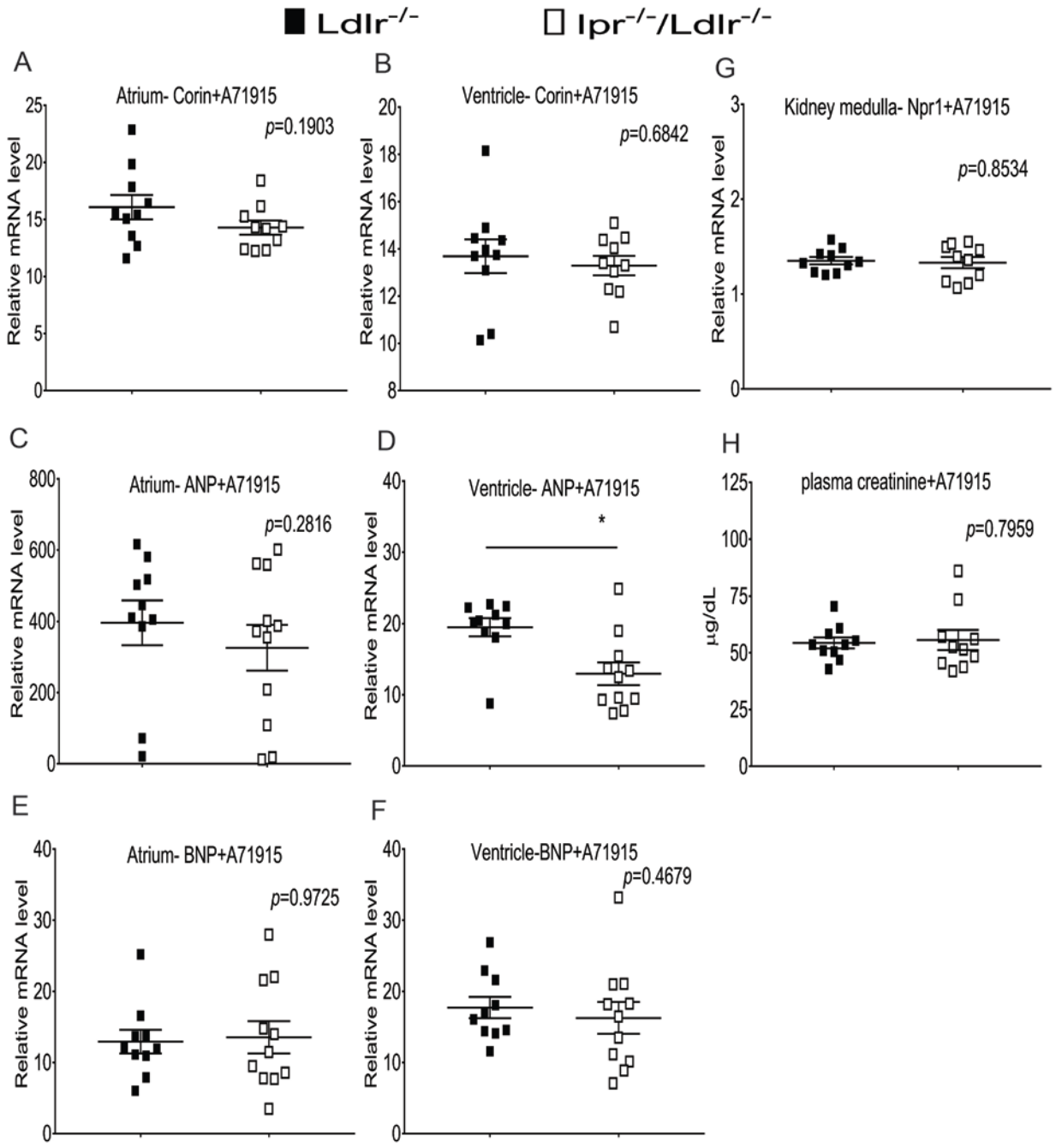

Supplemental Figure 13. Blockade of the ANP receptor with A71915 abolished the differences in corin, ANP and BNP transcripts in heart atrium and ventricle and Npr1 in kidney medulla between male Ipr$^{-/-}$/Ldlr$^{-/-}$ and Ldlr$^{-/-}$ mice, as measured by RT-qPCR.

Heart atrium, heart ventricle and kidney medulla tissue samples were dissected and RNAs were

extracted from $Ldlr^{-/-}$ and $Ipr^{-/-}/Ldlr^{-/-}$ mice fed an HSD for two weeks in conjunction with ANP inhibition via A71915 infusion (50μg/Kg BW/day) were used for real-time PCR analyses as described in the Methods. Plasma level of creatinine was measured by LC-MS as an indicator of kidney function in mice administered with A71915. No significant differences were detected in corin (A&B), ANP (C), BNP (E&F) and Npr1 (G) transcripts and plasma creatinine levels (H) between $Ldlr^{-/-}$ and $Ipr^{-/-}/Ldlr^{-/-}$ mice. Ventricle ANP transcript was significantly reduced in $Ipr^{-/-}/Ldlr^{-/-}$ compared with $Ldlr^{-/-}$ mice (D). Data are expressed as means ± SEMs (Parametric test, two-tailed, $*p < 0.05$; n=10 per genotype).

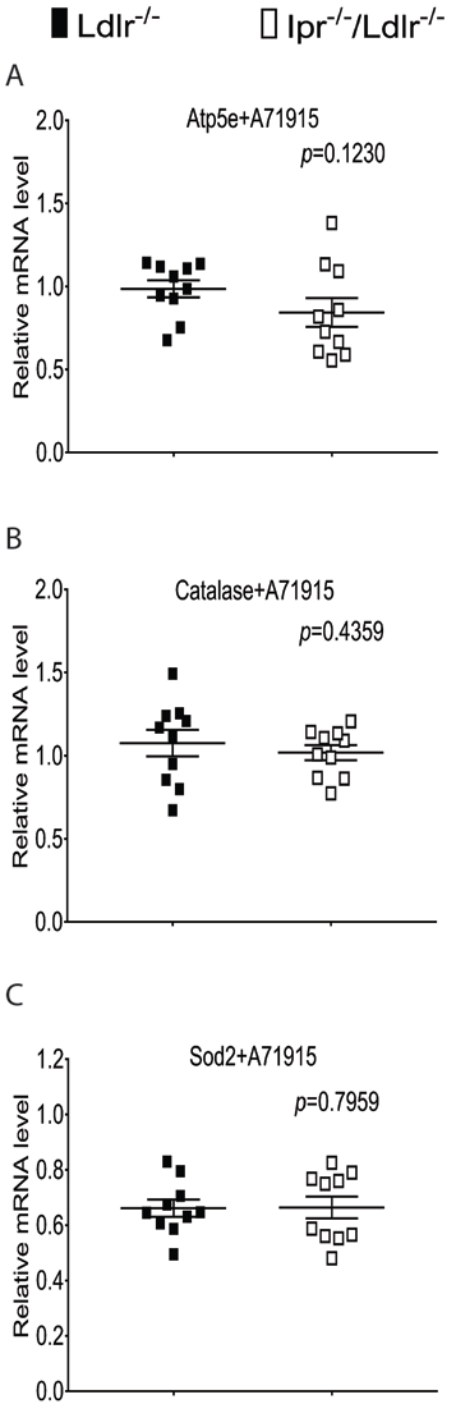

Supplemental Figure 14. Blockade of the ANP receptor with A71915 abolished the genotype dependent differences in mitochondrial dysfunction and oxidative phosphorylation pathway transcripts in kidney medulla of male mice, as measured by RT-

qPCR. RNA samples isolated from kidney medulla of Ldlr$^{-/-}$ and Ipr$^{-/-}$/Ldlr$^{-/-}$ mice after two weeks on an HSD in conjunction with ANP inhibition via A71915 infusion (50µg/Kg BW/day) were used for real-time PCR analyses. No significant differences in Atp5e (A), catalase (B) and Sod2 (C) were observed between Ldlr$^{-/-}$ and Ipr$^{-/-}$/Ldlr$^{-/-}$ mice. Data are expressed as means ± SEMs (Parametric test, two-tailed, p> 0.05; n=10 per genotype).

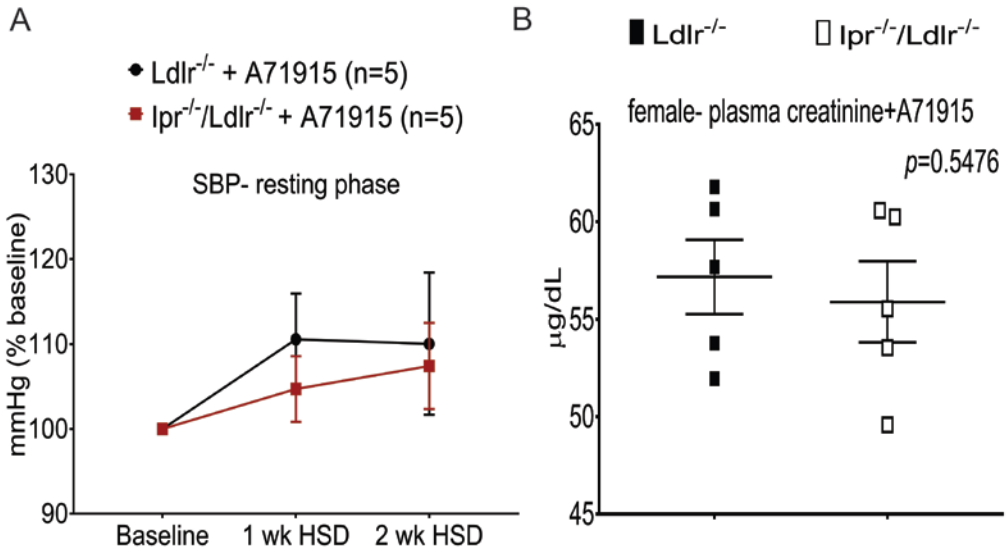

Supplemental Figure 15. Deletion of Ipr did not alter systolic blood pressure and plasma creatinine in female mice fed a high salt diet in conjunction with an ANP receptor antagonist. (A) The atrial natriuretic peptide receptor antagonist (A71915, 50µg/Kg BW/day) did not alter SBPs in female Ip-deficient hyperlipidemic mice. A71915 was delivered via mini-pumps and BPs was measured using a tail-cuff system before, one and two weeks after feeding a HSD. Two-way ANOVA revealed no significant effect of feeding time and genotype on SBP in Ldlr$^{-/-}$ and Ipr$^{-/-}$/Ldlr$^{-/-}$ mice. Data are expressed as means ± SEMs. p> 0.05; n=5 per genotype. (B) Plasma creatinine level was measured by LC-MS as described in the Methods. Deletion of Ip

did not significantly alter plasma creatinine compared with Ldlr$^{-/-}$ littermates fed an HSD+ A71915 for two weeks. Data are expressed as means ± SEMs (Parametric test, two-tailed, $p > 0.05$; n=5 per genotype).

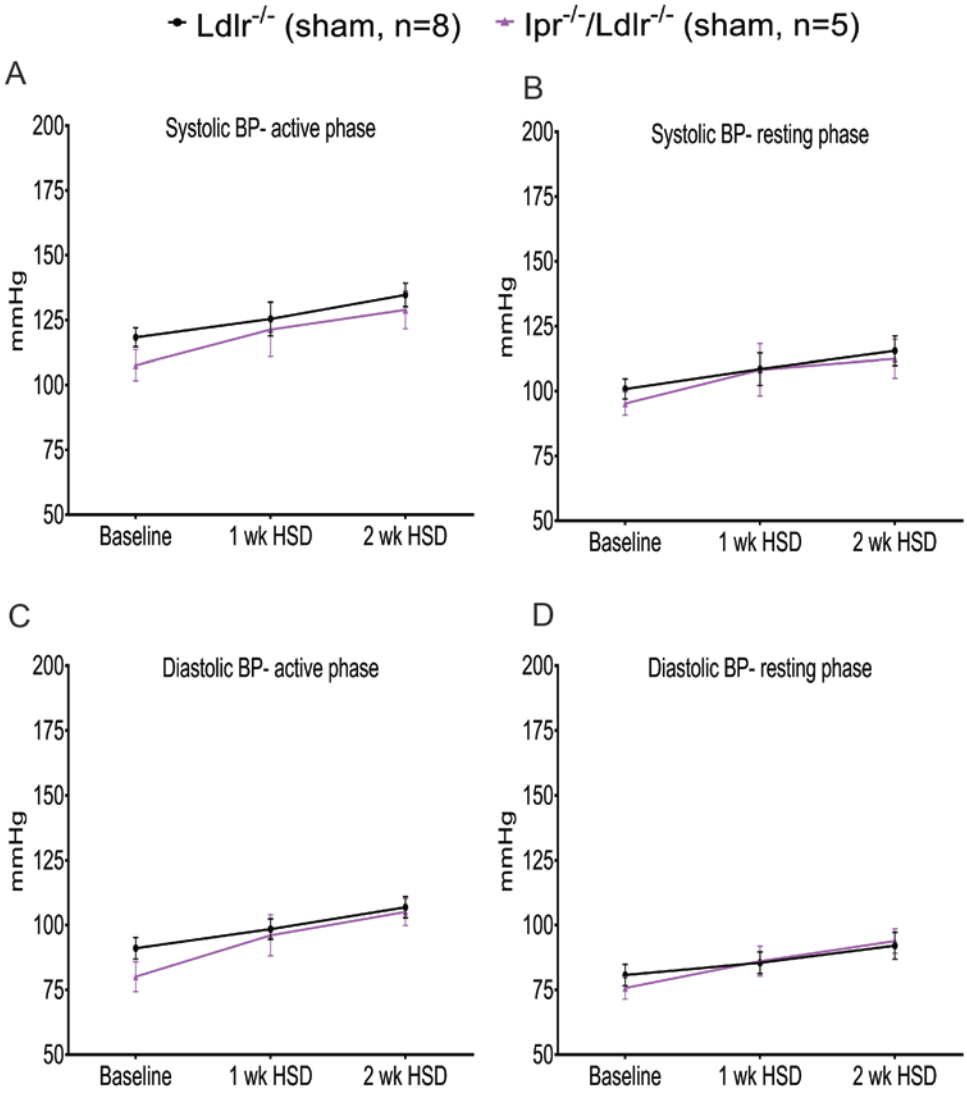

Supplemental Figure 16. High salt diet failed to alter BP responses in female sham-operated Ldlr$^{-/-}$ and Ipr$^{-/-}$/Ldlr$^{-/-}$ mice. Salt loading did not significantly alter SBP (A-B) and DBP (C-D) of sham-operated Ipr$^{-/-}$/Ldlr$^{-/-}$ compared with Ldlr$^{-/-}$ mice. Two-way ANOVA

revealed no significant effect of genotype and feeding time on SBP and DBP (p> 0.05). Data are expressed as means ± SEMs. n=5- 8 per genotype.

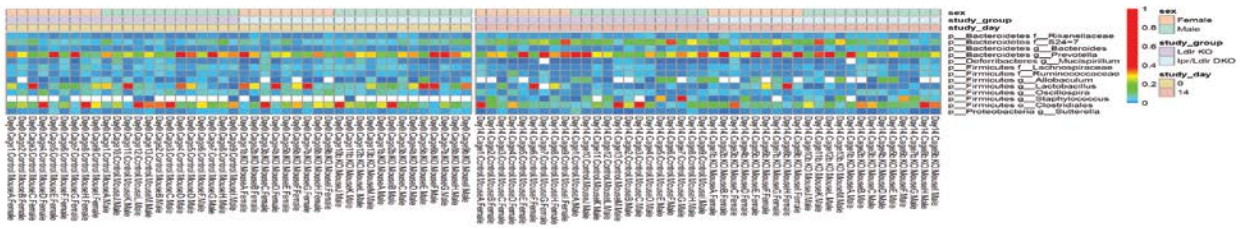

Supplemental Figure 17. Heatmap of gut microbiota composition in a salt-evoked hypertension mouse model. The taxonomic identities of prominent OTUs (mean relative abundance among all parameters of >0.5%) are presented.

A

Alpha diversity

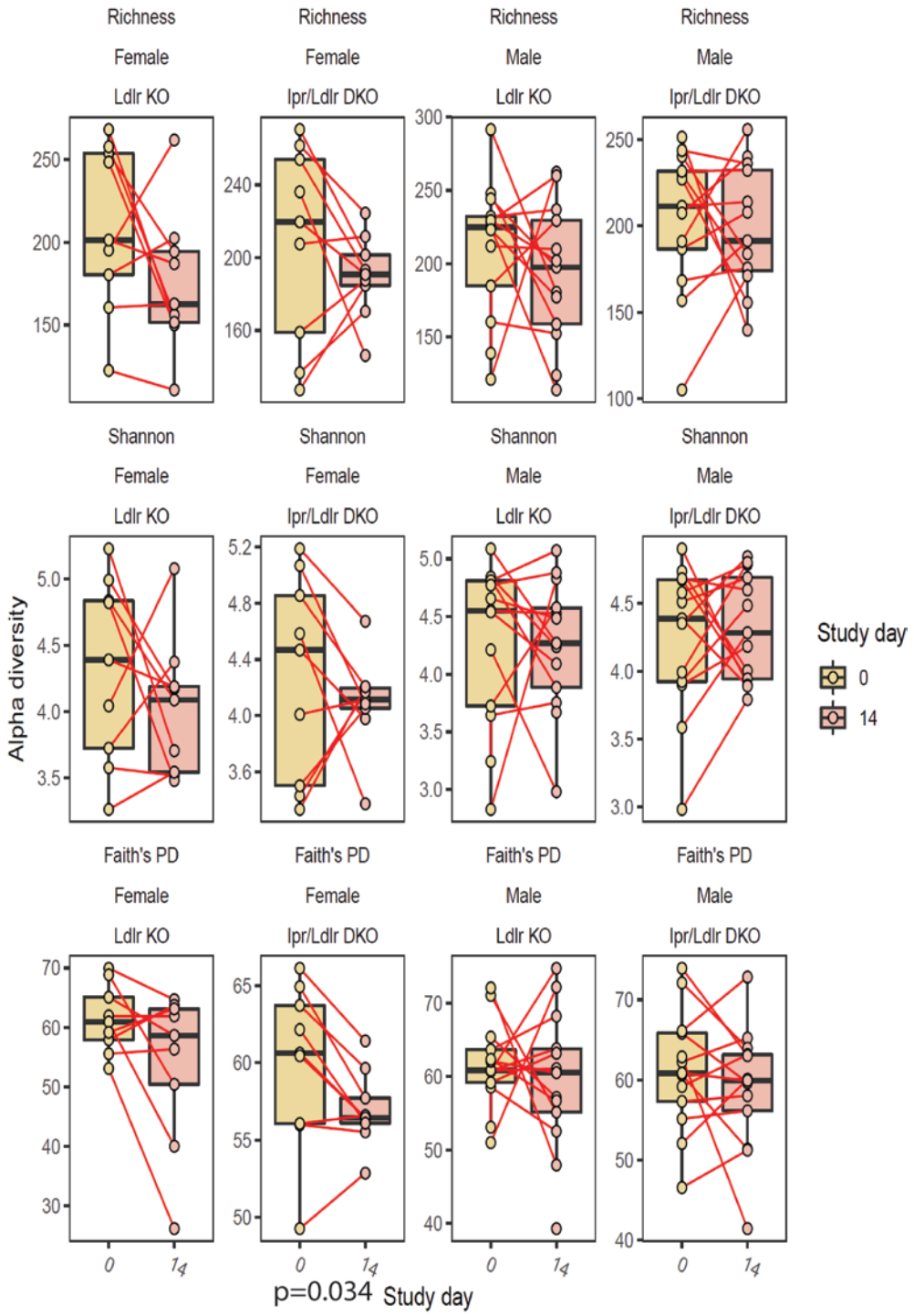

B

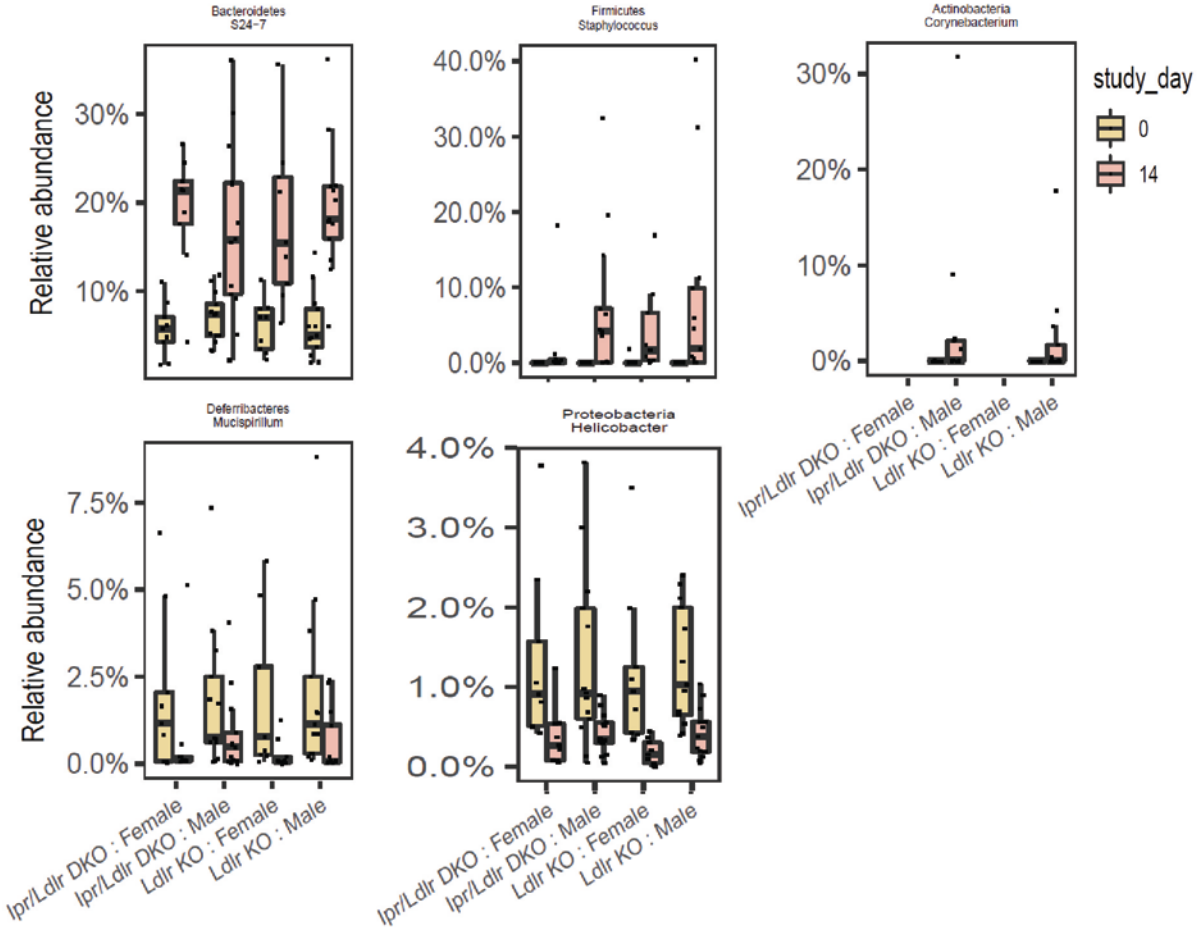
Bacteroidetes
S24-7
Firmicutes
Staphylococcus
Actinobacteria
Corynebacterium
Deferribacteres
Mucispirillum
Proteobacteria
Helicobacter
Relative abundance
study_day
0
14
Ipr/Ldlr DKO : Female
Ipr/Ldlr DKO : Male
Ldlr KO : Female
Ldlr KO : Male

C **Alpha diversity**

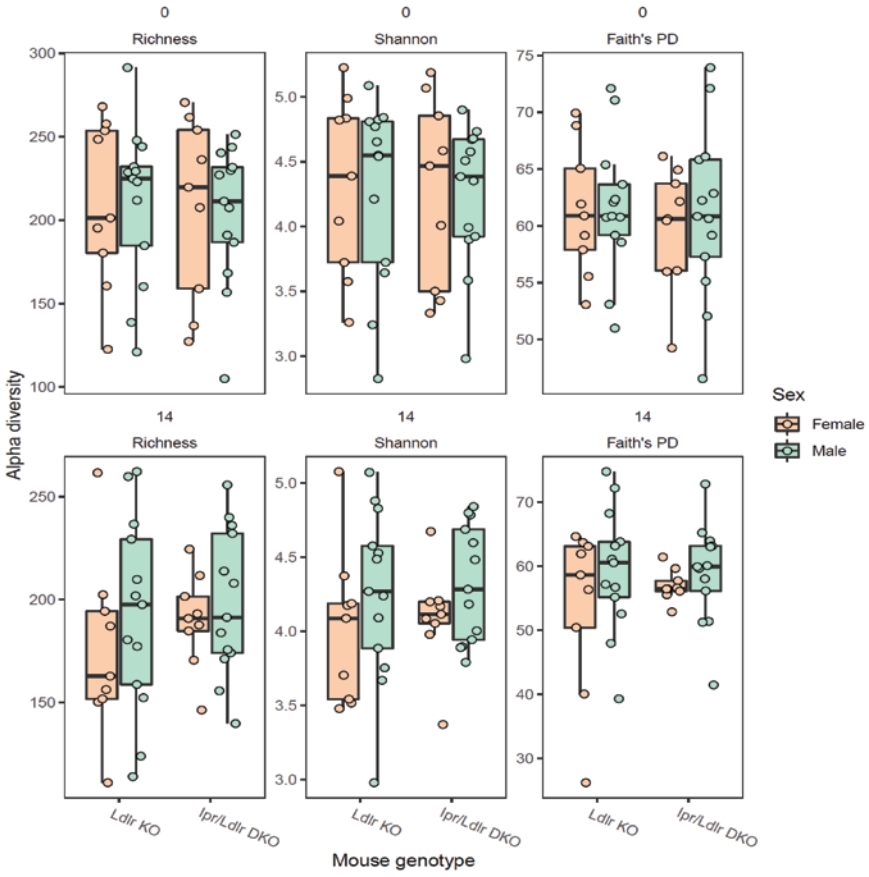

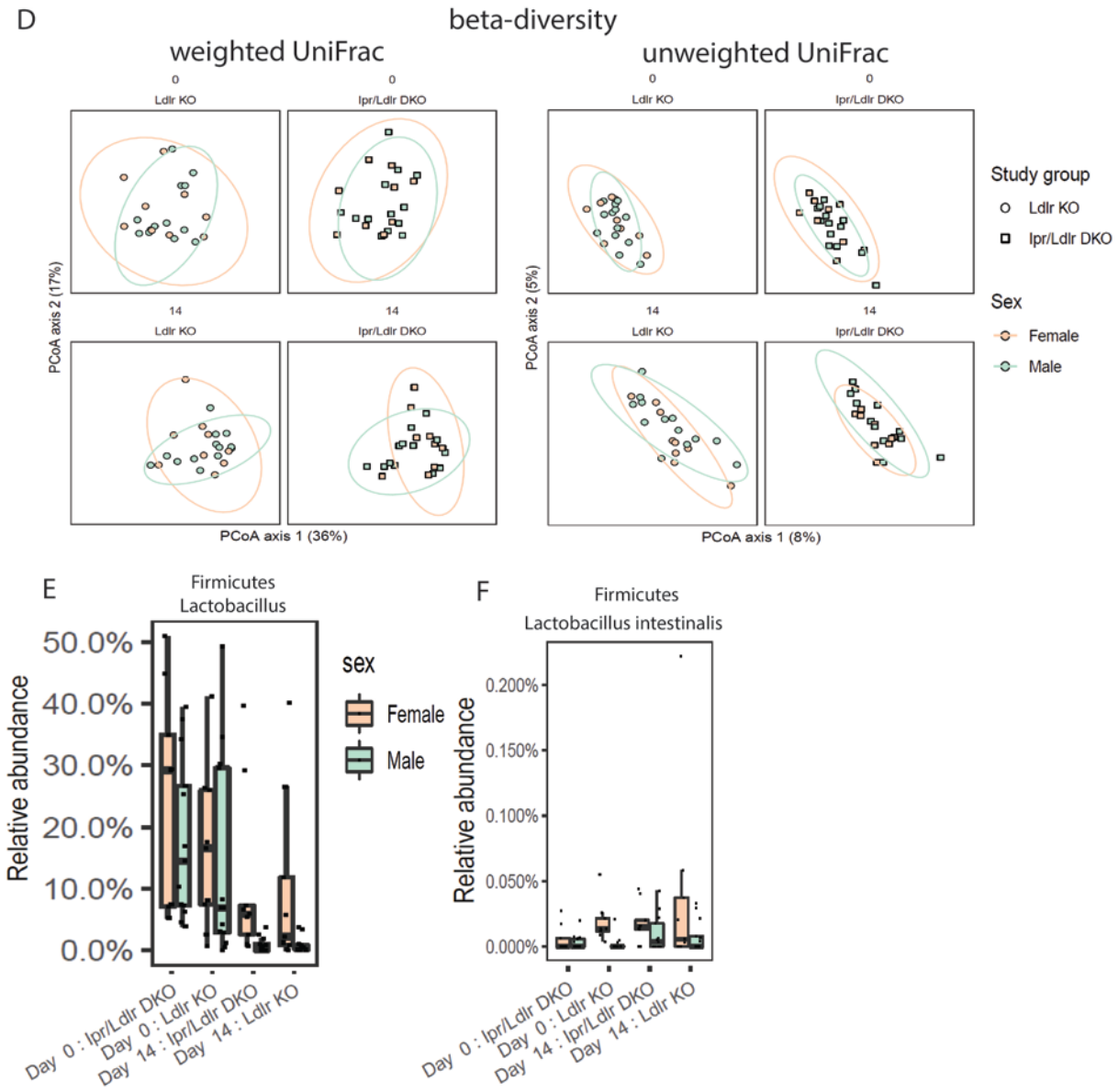

Supplemental Figure 18. HSD alters gut microbiota composition. Fecal pellets were collected from singly housed mice at baseline (day 0) and 2 weeks (day 14) after feeding a HSD. Bacterial DNA was extracted and analyzed by 16S rRNA marker gene sequencing. (A) α-diversity of microbiota was measured by Richness, Shannon and Faith's PD metrics. For comparison between day 0 and day 14, α-diversity by Faith's PD revealed a significant difference in female

Ipr$^{-/-}$/Ldlr$^{-/-}$ (Ipr/Ldlr DKO) mice at day 14. (B) Several OTUs were significantly increased regardless of the sex or genotypes of mice at day 14, including species of the family *Bacteroidales S24-7* and genera *Staphylococcus*, while *Mucispirillum* and *Helicobacter* decreased. *Corynebacterium* was detected only in male mice and significantly increased after a HSD feeding. (C) There was no significant difference in α-diversity between female and male mice regardless of genotypes. (D) β-diversity of microbiota was significantly different between female and male Ldlr$^{-/-}$ (Ldlr KO) mice at day 0 and Ipr$^{-/-}$/Ldlr$^{-/-}$ mice at day 14 (unweighted UniFrac). (E) At day 14, there was a significant decrease in *Lactobacillus* (p= 0.03) in male Ipr/ Ldlr$^{-/-}$ mice. (F) Species type strains showed a significant decrease of *Lactobacillus intestinalis* (p= 1.6x10^{-4}) in male Ldlr$^{-/-}$ mice compared with female mice.

A

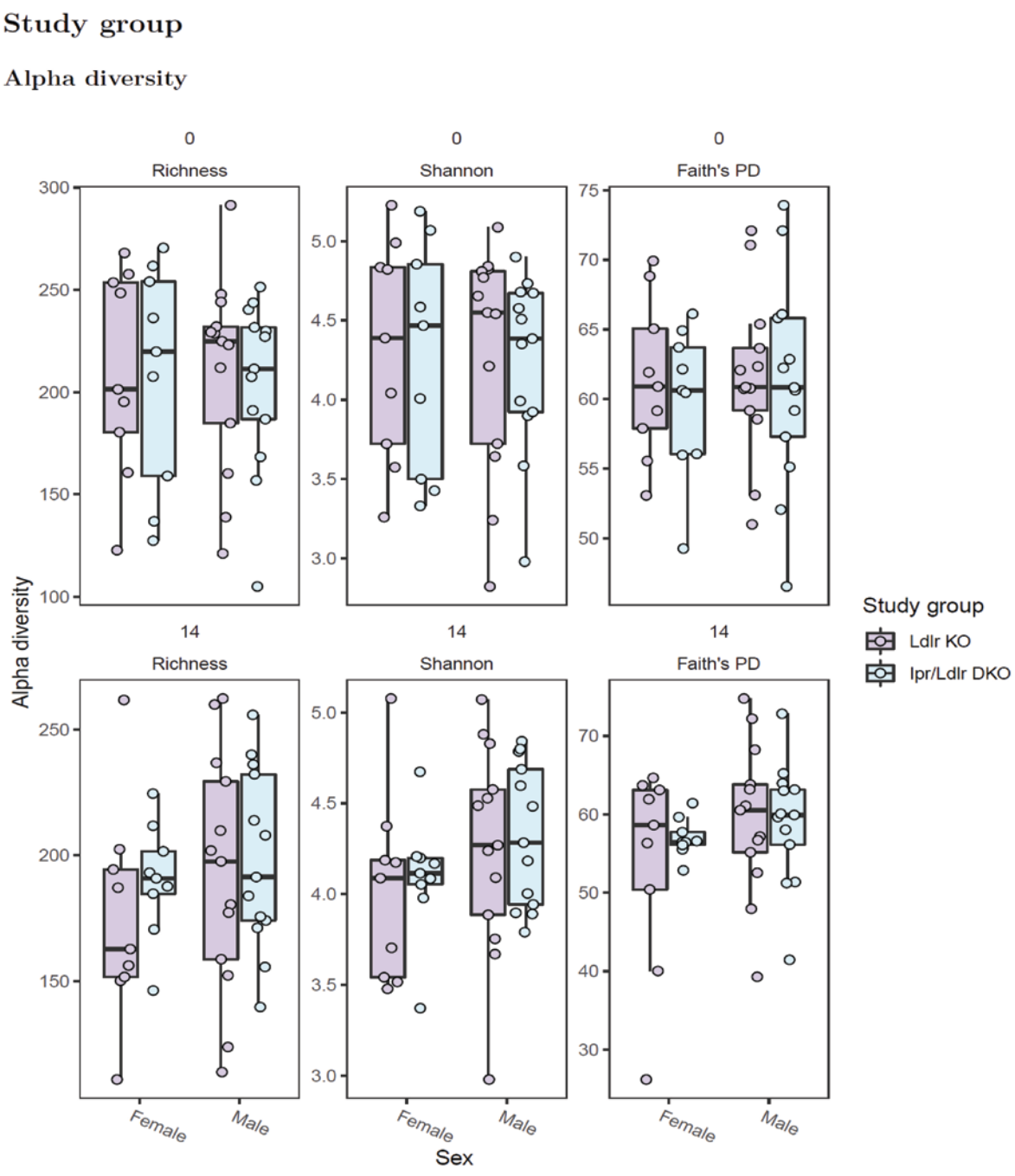
Study group
Alpha diversity
0
Richness
Shannon
Faith's PD
14
Alpha diversity
Female
Male
Sex
Study group
Ldlr KO
Ipr/Ldlr DKO

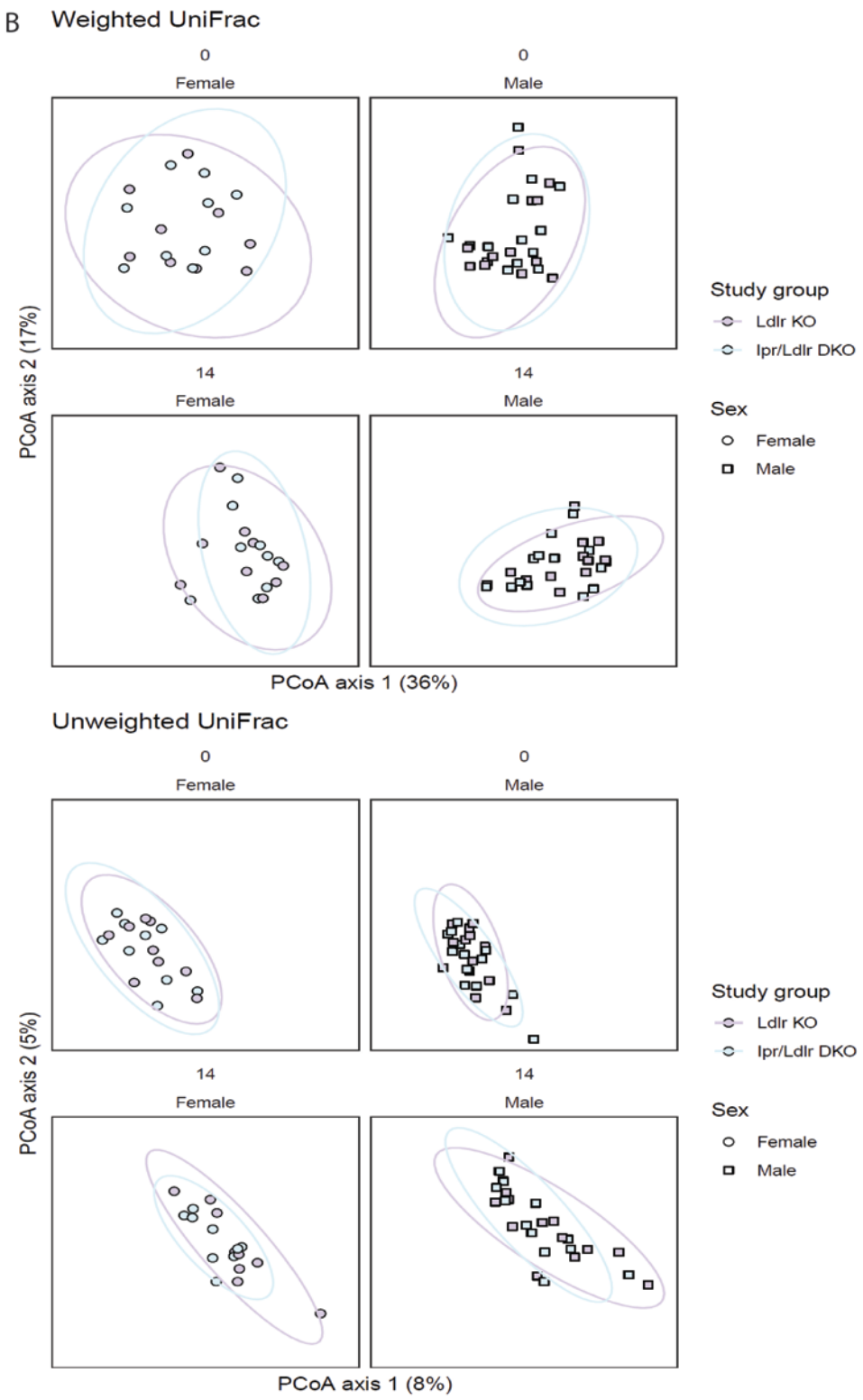

Supplemental Figure 19. Ipr deletion did not alter HSD-induced changes in gut microbiota composition. (A) α-diversity and (B) β-diversity measures were not significantly altered

between Ldlr$^{-/-}$ and Ipr$^{-/-}$/ Ldlr$^{-/-}$ mice (study group) at day 0 or day 14 in both female and male mice.

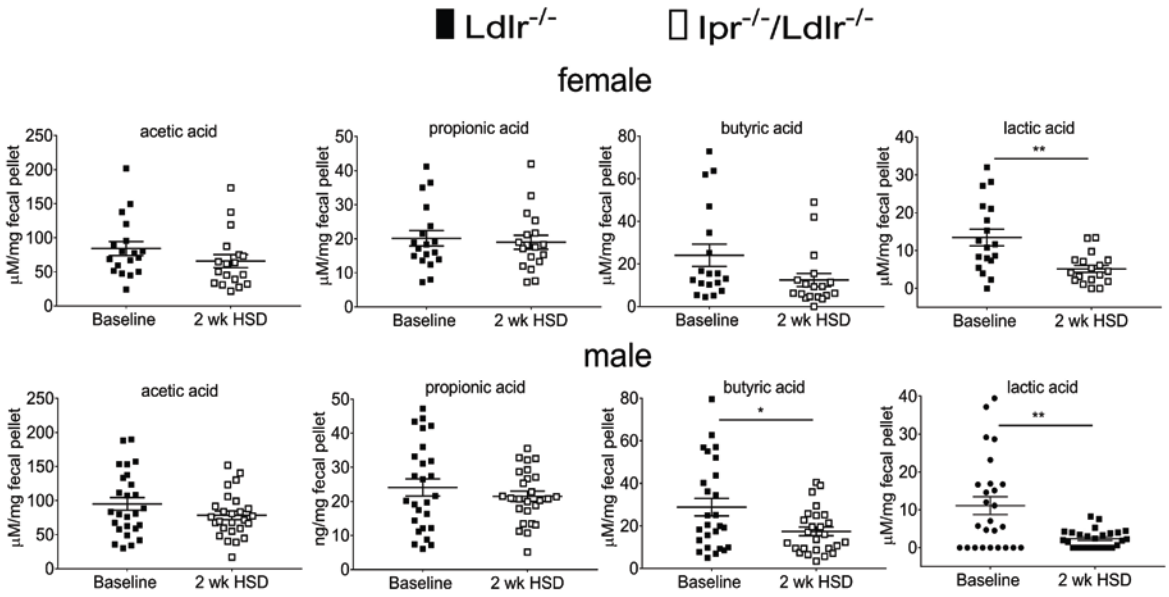

Supplemental Figure 20. HSD alters microbiota-derived fecal short-chain fatty acids. Fecal pellets were collected from singly housed mice at baseline and 2 weeks after feeding a HSD. Fecal metabolites were extracted with D_2O and short-chain fatty acids were analyzed by ^1H NMR. HSD significantly decreased levels of lactic acid in female (A) and male mice (B). The decrease in butyric acid was significant only in male mice. Both acetic acid and propionic acid were not altered between baseline and 2 weeks after HSD. Data are expressed as means ± SEMs (Parametric test, paired, two-tailed, *p< 0.05, **p< 0.01; female n= 18, male n= 26 male per genotype).

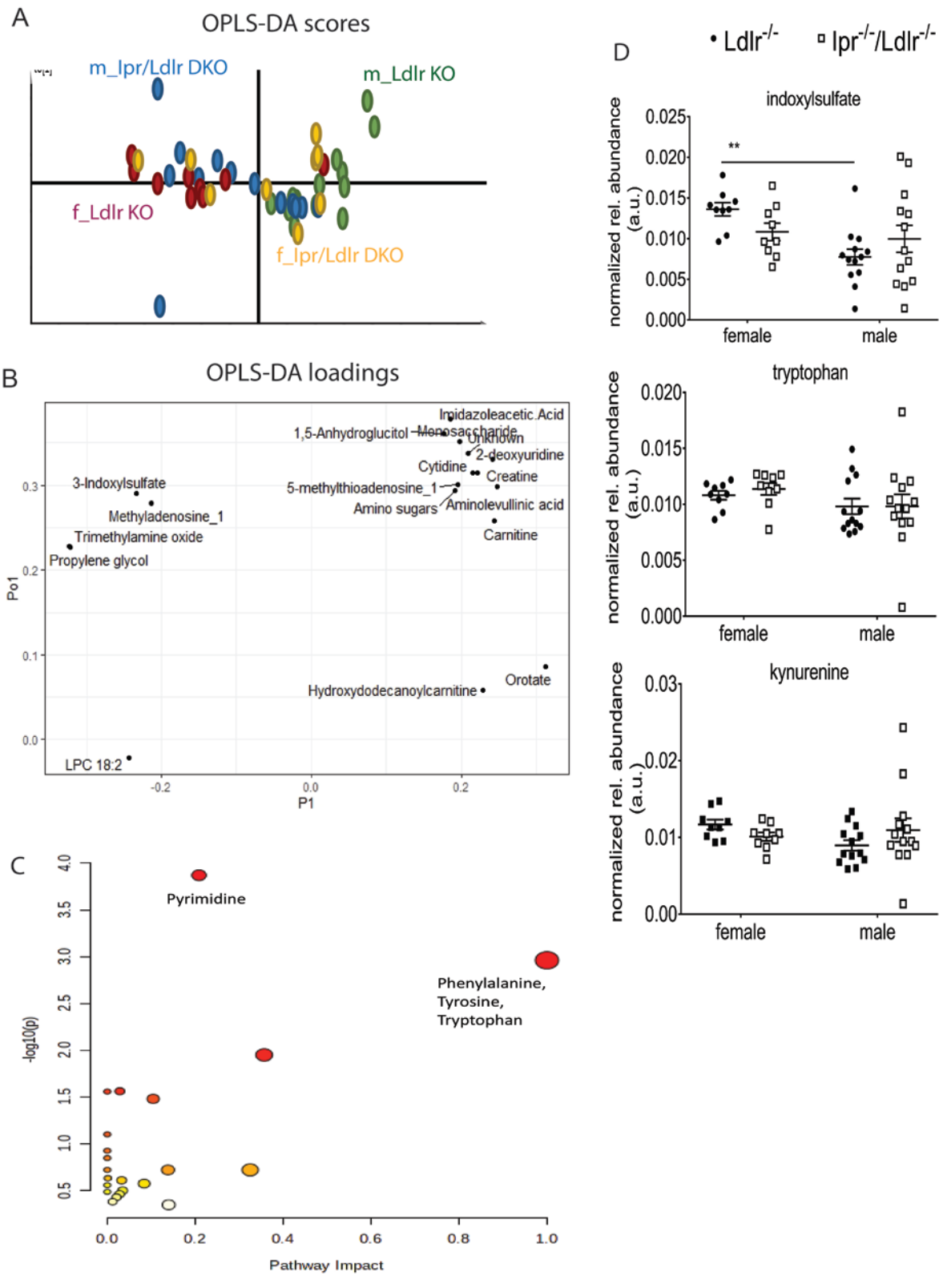
A
OPLS-DA scores
m_Ipr/Ldlr DKO
m_Ldlr KO
f_Ldlr KO
f_Ipr/Ldlr DKO
B
OPLS-DA loadings
Imidazoleacetic Acid
1,5-Anhydroglucitol
Monosaccharide
Unknown
2-deoxyuridine
Cytidine
Creatine
3-Indoxylsulfate
5-methylthioadenosine_1
Amino sugars
Aminolevullinic acid
Methyladenosine_1
Carnitine
Trimethylamine oxide
Propylene glycol
Orotate
Hydroxydodecanoylcarnitine
LPC 18:2
Po1
P1
C
Pyrimidine
Phenylalanine,
Tyrosine,
Tryptophan
-log10(p)
Pathway Impact
D
• Ldlr-/-
▫ Ipr-/-/Ldlr-/-
indoxylsulfate
tryptophan
kynurenine
normalized rel. abundance (a.u.)
female
male
**

Supplemental Figure 21. HSD alters plasma metabolites between female and male Ldlr$^{-/-}$ mice. Plasma samples were collected from mice on a HSD for two weeks. 50µl of plasma was dried and reconstituted with acetonitrile: water (50% v/v) for metabolomics analysis by UPLC-MS/MS. (A) OPLS-DA analysis revealed a distinct separation between female Ldlr$^{-/-}$ (red spheres) and male Ldlr$^{-/-}$ (green spheres) mice. (B) Plasma levels of indoxyl sulfate, methyladenosine, trimethylamine oxide and propylene glycol were reduced in male Ldlr$^{-/-}$ mice compared with female Ldlr$^{-/-}$ mice in OPLS-DA loading plot. Metabolites such as deoxyuridine, cytidine, orotate, etc on the right side (P1> 0) of the plot were increased in male Ldlr$^{-/-}$ mice. (C) MetaboAnalyst revealed several metabolic pathways were impacted by feeding a HSD, especially amino acid metabolism. (D) HSD significantly decreased plasma indoxyl sulfate in male Ldlr$^{-/-}$ compared with female Ldlr$^{-/-}$ mice. Plasma tryptophan and kynurenine levels were not altered. Two-way ANOVA showed a significant effect of sex on plasma levels of indoxyl sulfate in Ldlr$^{-/-}$ mice. Sidak's multiple comparison tests were used to test significant differences between sexes. Data are expressed as means ± SEMs, $^{**}p < 0.01$, female n= 9, male n= 13 per genotype).

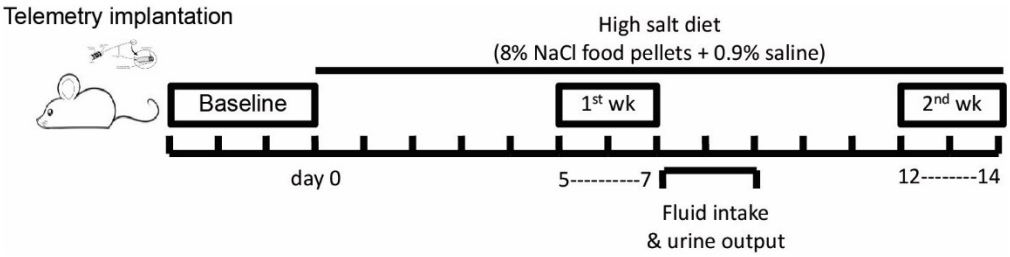

Supplemental Figure 22. Experimental protocol for the high salt diet regimen. Eight-to-ten week old mice were implanted with a telemetry transmitter and allowed to recover for at least five days. Baseline blood pressures (SBP and DBP) was recorded for three days before they were placed on a high salt diet (HSD, 8% NaCl+0.9% saline) for two weeks. The recoding system was switched on again from day 5- 7 and day 12-14. Urinary output and fluid intake were estimated by transferring mice into metabolic cages one week after the HSD. Fluid and foods were provided *ad libitum* during the experimental period. At the end of two weeks, mice were sacrificed and plasma and tissues were collected for analyses.

Sex dependent compensatory mechanisms preserve blood pressure homeostasis in prostacyclin receptor deficient mice

[1]Soon Yew Tang, PhD; [1]Hu Meng, PhD, [1]Seán T. Anderson, PhD; [1]Dimitra Sarantopoulou, MSc; [1]Soumita Ghosh, PhD; [1]Nicholas F. Lahens, PhD; [1]Katherine N. Theken, [1]Emanuela Ricciotti, PhD; [1]Elizabeth J. Hennessy, PhD; [2]Vincent Tu, PhD; [2]Kyle Bittinger, PhD; [1]Aalim Weiljie, PhD; [1-3]Gregory R. Grant, PhD; [1]*Garret A. FitzGerald, MD

[1]From the Institute for Translational Medicine and Therapeutics, Department of Systems Pharmacology and Translational Therapeutics, Perelman School of Medicine, University of Pennsylvania, Philadelphia, Pennsylvania, USA., [2]Division of Gastroenterology, Hepatology, and Nutrition, Children's Hospital of Philadelphia, Philadelphia, Pennsylvania, USA. [3]Department of Genetics, University of Pennsylvania, Philadelphia, Pennsylvania, USA.

[1]*Garret A. FitzGerald, MD

[1]From the Institute for Translational Medicine and Therapeutics, Perelman School of Medicine, Department of Systems Pharmacology and Translational Therapeutics, [2]Department of Genetics, University of Pennsylvania, Philadelphia, Pennsylvania, 19104-5127. [3]Current address at National Institute on Aging, National Institutes of Health, 21224.

*Address for correspondence: Garret A. FitzGerald, Institute for Translational Medicine and Therapeutics, Perelman School of Medicine, 10-110 Smilow Center for Translational Research, 3400 Civic Center Blvd, Bldg 421, University of Pennsylvania, Philadelphia, PA 19104-5158. Fax: 215-573-9135 Tel: 215-898-1184 Email: garret@upenn.edu

Subject code: Vascular Disease

Supplemental Methods

Generation of Ipr$^{-/-}$ and mPges-1$^{-/-}$ hyperlipidemic mice

All animals used in this study were on C57BL/6 background and housed individually. Ipr$^{-/-}$ and mPges-1$^{-/-}$ mice were generated on a hyperlipidemic background by crossing them with mice lacking the low-density lipoprotein receptor (Ldlr$^{-/-}$ - Jackson Laboratory) that were inter-crossed to breed Ipr $^{+/-}$/mPges-1 $^{+/-}$/Ldlr$^{-/-}$ mice. The heterozygous mice were intercrossed to produce Ldlr$^{-/-}$, Ipr$^{-/-}$/Ldlr$^{-/-}$, mPges-1$^{-/-}$/Ldlr$^{-/-}$, and Ipr$^{-/-}$/mPges-1$^{-/-}$/Ldlr$^{-/-}$ mice. Loss of Ipr, mPges-1 and Ldlr alleles were assessed by PCR analyses. Single nucleotide polymorphism (SNP) analyses showed that our mouse models achieved at least 97% purity on the C57BL/6 background. Mice of both sexes were fed a high salt diet (HSD, 8% NaCl, 5.3% fat, TD.92012, Harlan Teklad, Madison, WI) and saline containing 0.9% NaCl (Hospira, Lake Forest, IL) from 8-10 weeks of age for two weeks. Mice were weighed before and after the HSD feeding.

Blood pressure measurement using radio telemetry

Continuous 24-h systolic and diastolic BPs were monitored in free running mice with the Dataquest IV systems (Data Science) as described previously.(1) Eight to ten weeks old mice were used in this experiment. Briefly, after recovering from surgery, mice were kept in a 12-hour light/ dark cycle and fed a normal chow diet (0.6% NaCl). During that time, baseline systolic and diastolic BPs, heart rate and locomotor activity of mice were measured continuously for 2-3 days. After switching to a HSD, BP was again measured continuously from day 5-7 and from day 12-14. All data are expressed as averages of 12-h day or 12-h night recordings (Supplemental Figure 22).

Fluid intake and urinary output

One week after HSD feeding, mice were housed in metabolic cages starting from 7 am for habituation in a 12-h light/ dark cycle housing facility. At 7 pm, fluid intake and urine production were recorded every 12-h for 48 hours while HSD and saline were provided *ad libitum*. Urine samples were pooled and reported as ml/g BW/day. An enrichment toy (2) was provided in each cage during the entire period.

Blood pressure measurement using at tail-cuff system during HSD administration with an atrial natriuretic peptide receptor antagonist (A71915)

SBP was measured in conscious mice using a computerized, non-invasive tail-cuff system (Visitech Systems, Apex, NC) as described (3, 4). In male mice, BP was recorded twice each day from 7 to 9 am and 7 to 9 pm for 2-3 consecutive days after 3 days of training. In female mice, BP was recorded once each day from 7 to 9 am for 3 consecutive days after 3 days of training. Averaged SBPs were reported. Atrial natriuretic peptide receptor antagonist (A71915, 50μg/Kg BW/day, H-3048, Bachem California, Torrance, CA) was dissolved in saline and delivered via minipumps in mice during HSD feeding period. A71915 was shown to inhibit cGMP response by 3 orders of magnitude in *in vitro* studies (5) and attenuated hypertension and cardiac hypertrophy in 2K1C rats with prolonged exposure to nimesulide or NS-398 (COX-2 inhibitors) via the activation of ANP signaling pathway (6).

Pharmacological inhibition of mPGES-1 enzyme in humanized mPges-1 hyperlipidemic mice

Male mice with knock in of human mPges-1 were crossed with Ldlr$^{-/-}$ mice and commenced at 8 weeks of age were fed a high fat diet (Harlan Teklad, TD 88137) for 39 weeks alone and in combination with a specific inhibitor of mPGES-1 (MF970, 10 mg/ Kg BW; a kind gift of Merck). BP was measured using the tail-cuff system as mentioned. Urinary prostanoid

metabolites were measured by liquid chromatography/ mass spectrometry as described. Most pharmacological inhibitors of human mPGES-1 fail to engage the murine enzyme (7).

Mass spectrometric analysis of prostanoids and isoprostanes

Urinary prostanoid metabolites were measured by liquid chromatography / mass spectrometry as described (8). Such measurements provide a noninvasive, time integrated measurement of systemic prostanoid biosynthesis (9). Briefly, mouse urine samples were collected using metabolic cages over an 8 hour period (9am to 5pm). Systemic production of PGI_2, PGE_2, PGD_2, and TxA_2 was determined by quantifying their major urinary metabolites- 2, 3-dinor 6-keto $PGF_{1\alpha}$ (PGIM), 7-hydroxy-5, 11-diketotetranorprostane-1, 16-dioic acid (PGEM), 11, 15-dioxo-9α-hydroxy-2, 3, 4, 5-tetranorprostan-1, 20-dioic acid (tetranor PGDM) and 2, 3-dinor TxB_2 (TxM), respectively. For isoprostanes (iPs), the most abundant iPs detected in urine, 8,12-*iso*-$iPF_{2\alpha}$-VI was measured (10). Results were normalized with urinary creatinine.

Mass spectrometric analysis of plasma or urinary creatinine

Quantitation of plasma or urinary creatinine was performed using ultra high pressure liquid chromatography/tandem mass spectrometry (UPLC/MS/MS) with positive electrospray ionization and multiple reaction monitoring. A stable isotope-labeled internal standard (0.1mL for plasma, 1mL for urine, 2.5µg/mL [d3]-creatinine in 3% H_2O/acetonitrile) was added to 10µL of mouse plasma or urine. The resulting solution of urine samples was further diluted by 10 times. Samples were transferred into an autosampler vial and 20 µL was injected to the UPLC-MS/MS system. A Shimadzu Prominence UPLC system was used for chromatography. The UPLC column was a 2.1 x 50 mm with 2.5µm particles (Waters XBridge BEH HILIC). The mobile phase A was 100% acetonitrile. The mobile phase B was 5mM ammonium formate (pH = 3.98). The flow rate was 350µL/min. Separations were carried out with fixed solvent gradients

(12% mobile phase B). The Thermo Finnigan TSQ Quantum Ultra tandem instrument (Thermo Fisher Scientific) equipped with a triple quadrupole analyzer was operated in positive-mode ESI and the analyzer was set in the MRM mode for the analysis of creatinine. The transition for creatinine was 114>86. Quantitation was done by peak area ratio and results were normalized to the sample volume.

Urinary atrial natriuretic peptide, total nitrate+nitrite and sodium levels and plasma renin level

Atrial natriuretic peptide (Arbor Assays, K026-H1, Ann Arbor, MI), total nitrate+nitrite (Cayman Chemical, 780001, Ann Arbor, MI) and sodium (Biovision, K391-100, Milpitas, CA) levels in mouse urine and plasma renin levels (Abcam, ab138875, Cambridge, MA) were measured following manufacturer's instructions.

Preparation of mouse heart and kidney medulla for real-time PCR analysis of gene expression

Briefly, heart and kidney medulla were collected from animals perfused with ice-cold PBS dissolved in UltraPure™ DEPC-treated water to minimize degradation of RNA. The tissues were immediately stored separately in RNA*later*® solution (Ambion, Austin, TX) at 4°C. After 24h, the tissue samples were transferred to -80°C for storage until analyses. RNA was extracted using TRIzol® Reagent (Life Technologies, Grand Island, NY) and RNeasy Kit (Qiagen, Valencia, CA) following the manufacturer's protocol. The concentration and quality of extracted RNA from different tissues were measured using NanoDrop® 1000 (Thermo Scientific, Wilmington, DE) and reverse-transcribed into cDNA using Taqman Reverse Transcription Reagents (Applied Biosystems, Foster City, CA). Quantitative real time PCR was performed using Taqman Gene Expression Assays for ANP (Mm0125747_g1), BNP (Mm01255770_g1), Npr1 (Mm00435309_m1), Atp5e (Mm00445969_m1), Catalase (Mm00437992_m1), Sod2 (Mm00449726_m1), IL-17ra (Mm 00434214_m1), H2-M3 (Mm00469263_m1) and Foxp3

(Mm00475162_m1) using an ABI Prism 7900HT real-time PCR system in a 384 well plate. Results were normalized to HPRT (Mm01545399_m1).

Ovariectomy

Female mice at eight weeks old were bilaterally ovariectomized following procedures as described by Souza et al (11). For the 17β-estradiol (E2) study, mice recovered from the surgery were given E2 (150nM) in saline drinking fluid before feeding a HSD for 2 weeks. During the feeding period, the concentration of E2 was reduced to 100nM due to the increase in fluid consumption (12).

Haemotoxylin and eosin staining of kidney and aortic roots

Kidneys (n=4) and aortic roots (n=3) were formalin fixed and paraffin embedded, and 5 μm serial sections (6-10 sections) of the tissues were cut and mounted on Superfrost Plus slides for analysis of tissue morphology by HE staining.

RNA sequencing and analysis

Total RNA from mouse kidney medulla (16 samples- 8 males per genotype) and atria (36 samples- 9 males and 9 females per genotype) were isolated using Trizol and Qiagen RNeasy and RNA integrity was checked on an Agilent Technologies 2100 Bioanalyzer. RNA-seq libraries were prepared using the Illumina TruSeq stranded mRNA Library Prep Kit. The kidney samples were sequenced with an SBS Kit v3 on an Illumina HiSeq2500 (kidney) in a 2x150bp paired-end configuration, and the atria samples were sequenced on a NovaSeq 6000 (atria) using an S1 flow cell in a 2x100bp paired-end configuration. Samples were randomized and handled in a blinded fashion during sample preparation and sequencing. Ribosomal RNA was depleted using polyA selection as part of the standard sample preparation kit.

Raw RNA-seq reads were aligned to the GRCm38 build of the mouse genome by STAR v2.7.6a (13), with the following command line parameters: --outSAMunmapped Within KeepPairs--outFilterMismatchNmax33--seedSearchStartLmax33--alignSJoverhangMin 8. The kidney dataset contained an average of 15,480,386 sense and 74,242 antisense paired-end stranded 150bp reads mapping to genes, per sample. Data were normalized and quantified at both gene and exon-intron level, using a downsampling strategy implemented in the PORT pipeline (github.com/itmat/Normalization -v0.8.45e-beta). Both STAR and PORT were provided with gene models from release 102 of the Ensembl annotation (14). Differential expression analysis was performed in R v4.0.2 with v3.46.0 of the Limma voom package (15) to identify the most up or down regulated genes in the $Ipr^{-/-}$/$Ldlr^{-/-}$, compared to the $Ldlr^{-/-}$ mice, within each combination of gender and tissue. False Discovery Rate estimates were calculated using the Benjamini-Hochberg *p*-value correction. Enrichment analysis was done using the Ingenuity Knowledge Base (www.ingenuity.com). Pathway enrichment analyses were performed on the differential expressed genes (DEGs) with FDR < 0.12 (kidney medulla) and < 0.4 (atria). Data are deposited in Gene Expression Omnibus (NCBI) under accession number (GSE115916).

Fecal DNA purification, library preparation and sequencing

Bacterial DNA was extracted from fecal pellet (~20-40 mg) using the Qiagen DNeasy PowerSoil kit (Qiagen, Germantown, MD) and quantified with the Quant-iT PicoGreen Assay Kit (Thermo Fisher). 16S rRNA libraries were generated with barcoded PCR primers (27F 5′-AGAGTTTGATCCTGGCTCAG-3′ and 338R 5′-TGCTGCCTCCCGTAGGAGT-3′) annealing to the V1-V2 region (16). The PCR reactions were performed in quadruplicate using Q5 High-Fidelity DNA Polymerase (NEB, Ipswich, MA) and pooled together before purification using a 1:1 volume of SPRI beads (GE HealthCare, Chicago, IL). DNA of each sample was quantified

using Quant-iT PicoGreen Assay Kit (Thermo Fisher) and pooled in equal molar amounts. The final library was sequenced on the Illumina MiSeq (Illumina, San Diego, CA) using 2x250 bp chemistry. DNA free water, extraction blanks, and environmental controls were subjected to the same amplification and purification procedure to allow for empirical assessment of environmental and reagent contamination as negative controls. Eight artificial 16S gene fragments synthesized in gene blocks and combined in known abundances were included as positive controls (17).

Amplicon sequence processing

16S rRNA V1-V2 gene amplicon sequencing data were filtered for quality, de-multiplexed, and processed using the QIIME2 pipeline (18). Read pairs were subjected to quality control processing, chimeric sequence filtering, and identification of amplicon sequence variants (ASV) with DADA2 (19), implemented as a QIIME2 plugin. A total of 10,993 ASVs were found in the data set. Taxonomy of the ASV were assigned by classifying with the Greengenes reference database (20), using the naive Bayes classifier implemented in scikit-bio (21). After taxonomy assignment, the number of unique taxa went down to 130, and 19 (14.6%) of them were found with greater than 0.5% mean relative abundance across all samples and further analyzed for differential abundance. The unassigner software (https://github.com/kylebittinger/unassigner) ruled out species of Lactobacillus that were inconsistent with the ASV sequences and the remaining Lactobacillus species assignments were tested for differential abundance. Richness and Shannon indices as measurements of α-diversity were calculated and compared using the vegan package (version 2.5-7). To assess similarity between samples by weighted and unweighted UniFrac distances (22, 23), MAFFT (24) was used to align the sequences and highly variable positions were masked to reduce noise. Then, a mid-point rooted tree was generated

using FastTree (24) for calculating Faith's phylogenetic diversity and UniFrac distances. Global differences in bacterial community composition were visualized using Principal Coordinates Analysis (PCoA) using the ape package (version 5.4-1) in R with the UniFrac distances. The α-diversity and taxonomic profiles were visualized using the ggplot2 package (version 3.3.3).

Compositional statistical analysis

Community-level differences between sample groups were assessed using the PERMANOVA test in the vegan package (version 2.5-7), which uses sample-sample distances to test the null hypothesis of no difference in group centroid position [https://doi.org/10.1111/j.1442-9993.2001.01070.pp.x]. The significant differences of microbial taxa between sex, genotype, or study day was determined by modeling the log10 transformed relative abundance of each taxon using linear models (stats package) or linear mixed effects models (nlme package 3.1-151) with a random intercept for each subject. To correct for multiple comparisons, p values were adjusted using the method of Benjamini-Hochberg to control the false discovery rate (25). The level of significance was set at 5%.

Fecal metabolite extraction

Fecal samples (1 pellet, ~10-30 mg) were homogenized with Lysing Matrix E (MP Biomedicals) in 450 µl of heavy water (D_2O) using a Tissuelyser (Qiagen). Homogenized samples were centrifuged at 10,000 g for 10 min at 4°C and the supernatant was transferred to a new tube for second step of centrifugation at full speed. The supernatant was further filtered through a 0.22 µm centrifuge tube filter (Spin-X, cellulose acetate, Costar). 180 µl supernatant was transferred to a fresh tube for ^{1}H NMR analysis.

Fecal indole metabolite analysis by LC-MS/MS

Deuterated standard, [d2]- indole-3-acetic acid in acetonitrile (5 ng, 50 µL) was added to 150 µL of fecal supernatant, followed by diluting with 550 µL of acetonitrile containing 0.1% formic acid. Samples were vortexed and spun down at 21,000 g for 2 min. Clear supernatants were transferred to new tubes, dried under vacuum and reconstituted with 100 µL of 50% methanol. A 50 µL aliquot was injected into a C18 UPLC column (Waters ACQUITY UPLC CSH 2.1 × 50 mm × 1.7 µm) and eluted at a flow rate of 350 µL/ min with a linear gradient from 0% solvent B to 35% in 6.5 min. Mobile phase and MS parameters were optimized to obtain maximum sensitivity for detection of respective product ions. Mobile phase A was made of water: mobile phase B [95:5 (v/v)] with 65 mM ammonium acetate (pH 5.7); mobile phase B consisted of acetonitrile: methanol [95:5 (v/v)]. The analysis was performed on a Waters ACQUITY ultra-performance LC system in-line with a Waters Xevo TQ-S triple quadrupole mass spectrometer. The ultra-performance LC system directly interfaced with the positive-mode ESI source of the mass spectrometer using multiple reaction monitoring (MRM). Quantitation was done by two-point calibration (one is zero concentration point and another is mixture of 5 ng of indole-3-acetate acid, indole-3-lactic acid, indole-3-propionic acid standards) and results were normalized to sample volume and fecal mass. Quantitative Transitions of MRM method for each compound were 176 > 130 for indole-3-acetate acid, 178 > 132 for [d2]- indole-3-acetate acid, 206 > 118 for indole-3-lactic acid, and 190 > 130 for indole-3-propionic acid.

Short-chain fatty acid analysis by ^{1}H NMR

Fecal sample extracts were mixed with 20 µl of D_2O containing sodium trimethylsilypropanesulfonate (DSS) as NMR internal standard and then was transferred to 3mm NMR tube. ^{1}H NMR spectra were acquired in a 700 MHz Bruker Avance III HD NMR spectrometer (Bruker Biospin, Billerica, MA) fitted with a 3mm triple resonance inverse (TXI)

probe. All spectra were acquired using a NOESYPR1d pulse-program with relaxation delay of 1s, 0.1s mixing time, 76k data points and 14ppm spectral width. Presaturation technique during relaxation delay and mixing time to suppress water signal. Raw spectral data were imported into Chenomx v8.0 (Chenox Inc. Edmonton, Alberta, Canada) for further processing. The spectra were Fourier transformed after zero filling to 128k and applying linear broadening of 0.1 Hz. All spectra were referenced to internal standard followed by targeted profiling of metabolites of interest (26). The concentrations were further normalized to weights of fecal sample.

Plasma metabolomics

UPLC-MS/MS analysis was performed as reported previously (27). Briefly, dried plasma samples were reconstituted in 200 µl of acetonitrile: water (50% v/v) and 30 µl was transferred into mass spec vials (Phenomenex Inc. Torrance, CA). All samples were pooled to construct a quality control (QC) samples. All spectra were acquired using UPLC-ESI-QqQ-MS (Waters micro TQ-S, Waters Corp. Milford, MA) spectrometer. There were duplicate injections of 5 µl of reconstituted sample in randomized fashion. QC samples were run at regular interval throughout the run to correct for instrumental drift. Data was acquired in multiple reaction monitoring (MRM, developed in house) mode and was integrated using Waters Targetlynx 4.1 software. Every metabolite feature was fitted using a locally-weighted scatterplot smoothing (LOESS) function from the QC samples. Metabolites with 50% missing values and > 40% relative standard deviation were dropped. The data was further normalized with the probabilistic quotient normalization in R (28).

Statistical analysis

Statistical analyses of interactions between SBP/ DBP, genotypes, treatment week and phases in male hyperlipidemic mice. 4-way ANOVA with repeated measures and Greenhouse-Geisser

sphericity correction showed how SBP changes for different genotypes across time at active/inactive phase, where Ipr and mPges-1 are the between-subjects factors while week and phase are the repeated measures. ANOVA indicated that SBP is significantly affected by Ipr, mPges-1, phase, and the Ipr:week and week:phase interactions. The significant factors and interactions are listed below.

- Ipr, $F(1,54) = 17.2672925$, $p = 0.0001166$
- mPges1, $F(1,54) = 11.6363337$, $p = 0.0012316$
- phase, $F(1, 54) = 276.1276325$, $p = 0.0000000$
- Ipr:week, $F(2,108) = 10.0578885$, $p = 0.0005762$
- week:phase, $F(2,108) = 27.7076808$, $p = 0.0000000$

The week factor breaks the sphericity of the variances, so we performed a 3-way ANOVA with repeated measures to detect significant differences per week. The analysis showed that Ipr and mPges-1 state, as well as phase have significant effects on SBP across all weeks, while Ipr state and phase are interacting significantly only for week 1. We also tested for differences across the different genotypes by 2-way ANOVA with repeated measures and Greenhouse-Geisser correction. This restricted model indicates that when Ipr and mPges-1 are both knocked out, the phase and the phase:week interaction affect the SBP, whereas when they are both present, the week factor is also affecting the SBP. With Ipr knocked out only, phase significantly changes SBP, while with mPges-1 knock out, both week and phase significantly affect SPB.

Similarly, 4-way ANOVA with repeated measures and Greenhouse-Geisser sphericity correction showed how DBP changes for different genotypes across time at active/inactive phase, where Ipr and mPges-1 are the between-subjects factors while week and phase are the repeated measures.

ANOVA indicated that DBP is significantly affected by all four factors, and the Ipr:week and week:phase interactions. The significant factors and interactions are listed below.

- Ipr, $F(1,54) = 13.3603111$, $p = 0.0005829$
- mPges1, $F(1,54) = 7.8658849$, $p = 0.0069871$
- week, $F(2,108) = 4.1848207$, $p = 0.0241011$
- phase, $F(1, 54) = 121.9086652$, $p = 0.0000000$
- Ipr:week, $F(2,108) = 8.1299886$, $p = 0.0011381$
- week:phase, $F(2,108) = 12.5879864$, $p = 0.0000181$

A 3-way ANOVA with repeated measures was performed to detect the significant differences per week, and showed that Ipr and phase have significant effects on DBP across all weeks, with Ipr state and phase interacting significantly only at week 1. We also tested for differences across the different genotypes, by 2-way ANOVA with repeated measures and Greenhouse-Geisser correction. This restricted model indicates that phase and week:phase interaction affect the DBP in all genotypes, and when Ipr and mPges-1 are both present, the week factor has a significant effect on DBP as well. 2-way ANOVA with repeated measures for each pair of mPges-1 state and week indicates that when mPges-1 is knocked out, phase has a significant effect on DBP for all weeks. While when mPges-1 is present, the interaction of Ipr:phase is significant as well. This is also shown by 2-way ANOVA with repeated measures for each pair of mPges-1 state and phase that indicate that when mPges-1 is knocked out, a significant effect of Ipr and week is noticed during active phase only. When mPges-1 is present, Ipr state affects the DBP during resting phase, but during active phase DBP is affected by Ipr and Ipr:week interaction.

Statistical analyses of interactions among SBP/DBP, genotypes, treatment week and phases in female hyperlipidemic mice. 4-way ANOVA with repeated measures and Greenhouse-Geisser correction indicated that both SBP and DBP are significantly affected by phase (p=0) and the interaction week:phase (p=0). A 3-way ANOVA with repeated measures was performed to detect the significant differences per week, and showed that phase has significant effects on SBP and DBP across all weeks. We also tested for differences across the different genotypes, by 2-way ANOVA with repeated measures and Greenhouse-Geisser correction. This restricted model indicates that phase affects the SBP and DBP in all genotypes, and the week:phase interaction has a significant effect on DBP when Ipr is knocked out, and on SBP when either one or both of Ipr and mPges-1 are knocked out.

Statistical analyses of interactions among urinary prostaglandin metabolites, treatment week and genotypes. The 3-way ANOVA with repeated measures showed how prostaglandin biosynthesis changes for different genotypes with different treatments, and specifically that PGIM, PGDM and TxM excretion is significantly affected by mPges-1 presence or absence, whether the mice are on HSD or not and the interaction of these two factors, as shown below. PGEM biosynthesis is also affected by the interaction of the Ipr state and whether the mice are on HSD or not, as well as by the 3way interaction of mPges-1 state, Ipr state and whether the mice are on HSD or not.

For PGDM: mPges1, F(1,43)=77.4094975, p=0.00000000003620496, treatment, F(1,43)=5.5950815, p=0.02259109, mPges1:treatment, F(1,43)=4.6867501, p=0.03599118

For PGEM: mPges1, F(1,43)=67.30982657, p=0.0000000002439751, treatment, F(1,43)=5.02527221, p=0.03019348, Ipr:treatment, F(1,43)=4.69330814, p=0.03586802,

mPges1:treatment, F(1,43)=4.36810887, p=0.04256714, Ipr:mPges1:treatment, F(1,43)=9.25581947, p=0.003991717

For PGIM: mPges1, F(1,43)=60.09688, p=0.000000001066618, treatment, F(1,43)=29.3896179, p=0.000002522259, mPges1:treatment, F(1,43)=5.2963732, p=0.02627928

For TxM: mPges1, F(1,43)=16.21830969, p=0.0002254031, treatment, F(1,43)=29.70607333, p=0.000002289881, mPges1:treatment, F(1,43)=8.96320747, p=0.004553328

Statistical analysis of SBP with an ANP receptor antagonist (A71915) across time in male mice. 3-way ANOVA with repeated measures and Greenhouse-Geisser sphericity correction showed how SBP changes for different genotypes across time at active/inactive phase, where Ipr and A71915 are the between-subjects factors while week is the repeated measure. ANOVA indicated that SBP is significantly affected by Ipr, A71915 and week and the Ipr:week interaction at active phase, while in the resting phase there is additional significant effect of the A71915:week interaction. The significant factors and interactions are listed below.

Active phase:

- Ipr, F(1,32) = 10.172884, p = 3.182845e-03
- A71975, F(1,32) = 8.701888, p = 5.900875e-03
- week, F(2,64) = 0.9003809, p = 2.062779e-06
- Ipr:week, F(2,64) = 0.9003809, p = 2.885028e-02
- A71975:week, F(2,64) = 0.9003809, p = 3.188379e-02

Resting phase:

- Ipr, F(1,32) = 9.9083548, p = 3.549123e-03

- A71975, F(1,32) = 4.8523003, p = 3.492932e-02
- week, F(2,64) = 0.9043208, p = 1.383358e-07
- Ipr:week, F(2,64) = 0.9043208, p = 2.735816e-02

Statistical analyses of interactions between SBP, genotypes, treatment week and phases in ovariectomized female hyperlipidemic mice. 3-way ANOVA with repeated measures and Greenhouse-Geisser sphericity correction showed how SBP changes for different genotypes across time at active/inactive phase, where Ipr and E2 are the between-subjects factors while week is the repeated measure. ANOVA indicated that SBP is significantly affected by E2, week and the E2:week interaction at both active and resting phase. The significant factors and interactions are listed below.

Active phase:

- E2, F(1,26) = 8.3392931, p = 7.714758e-03
- week, F(2,52) = 0.6703226, p = 2.350992e-06
- E2:week, F(2,52) = 0.6703226, p = 1.078514e-02

Resting phase:

- E2, F(1,26) = 7.2338891, p = 1.232654e-02
- week, F(2,52) = 0.6998376, p = 0.0000250206
- E2:week, F(2,52) = 0.6998376, p = 0.0034673737

Statistical analyses of interactions between DBP, genotypes, treatment week and phases in ovariectomized female hyperlipidemic mice. 3-way ANOVA with repeated measures and Greenhouse-Geisser sphericity correction showed how DBP changes for different genotypes

across time at active/inactive phase, where Ipr and E2 are the between-subjects factors while week is the repeated measure. ANOVA indicated that DBP is significantly affected by week, and the Ipr:E2 and E2:week interactions at both active and resting phase. The significant factors and interactions are listed below.

Active phase:

- Ipr:E2, $F(1,26) = 5.46038554$, $p = 2.742940e-02$
- week, $F(2,52) = 0.6896006$, $p = 1.878692e-05$
- E2:week, $F(2,52) = 0.6896006$, $p = 1.229147e-02$

Resting phase:

- Ipr:E2, $F(1,26) = 5.954118$, $p = 2.180856e-02$
- week, $F(2,52) = 0.6714117$, $p = 4.303491e-05$
- E2:week, $F(2,52) = 0.6714117$, $p = 4.153677e-03$

References

1. Yu, Y., Ricciotti, E., Scalia, R., Tang, S.Y., Grant, G., Yu, Z., Landesberg, G., Crichton, I., Wu, W., Pure, E., et al. 2012. Vascular COX-2 modulates blood pressure and thrombosis in mice. *Sci Transl Med* 4:132ra154.
2. Key, D. 2004. Environmental enrichment options for laboratory rats and mice. *Lab Anim (NY)* 33:39-44.
3. Tang, S.Y., Monslow, J., G, R.G., Todd, L., Pawelzik, S.C., Chen, L., Lawson, J., Pure, E., and FitzGerald, G.A. 2016. Cardiovascular Consequences of Prostanoid I Receptor Deletion in Microsomal Prostaglandin E Synthase-1-Deficient Hyperlipidemic Mice. *Circulation* 134:328-338.
4. Cheng, Y., Wang, M., Yu, Y., Lawson, J., Funk, C.D., and Fitzgerald, G.A. 2006. Cyclooxygenases, microsomal prostaglandin E synthase-1, and cardiovascular function. *J Clin Invest* 116:1391-1399.

5. von Geldern, T.W., Budzik, G.P., Dillon, T.P., Holleman, W.H., Holst, M.A., Kiso, Y., Novosad, E.I., Opgenorth, T.J., Rockway, T.W., Thomas, A.M., et al. 1990. Atrial natriuretic peptide antagonists: biological evaluation and structural correlations. *Mol Pharmacol* 38:771-778.
6. Park, B.M., Gao, S., Cha, S.A., and Kim, S.H. 2015. Attenuation of renovascular hypertension by cyclooxygenase-2 inhibitor partly through ANP release. *Peptides* 69:1-8.
7. Berggvist F, M.R., Jakobsson PJ. 2019. A review on mPGES-1 inhibitors: From preclinical studies to clinical applications. *Prostaglandins Other Lipid Mediat.* 147:106383.
8. Song, W.L., Lawson, J.A., Wang, M., Zou, H., and FitzGerald, G.A. 2007. Noninvasive assessment of the role of cyclooxygenases in cardiovascular health: a detailed HPLC/MS/MS method. *Methods Enzymol* 433:51-72.
9. FitzGerald, G.A., Pedersen, A.K., and Patrono, C. 1983. Analysis of prostacyclin and thromboxane biosynthesis in cardiovascular disease. *Circulation* 67:1174-1177.
10. Lawson, J.A., Li, H., Rokach, J., Adiyaman, M., Hwang, S.W., Khanapure, S.P., and FitzGerald, G.A. 1998. Identification of two major F2 isoprostanes, 8,12-iso- and 5-epi-8, 12-iso-isoprostane F2alpha-VI, in human urine. *J Biol Chem* 273:29295-29301.
11. Souza, V.R., Mendes, E., Casaro, M., Antiorio, A., Oliveira, F.A., and Ferreira, C.M. 2019. Description of Ovariectomy Protocol in Mice. *Methods Mol Biol* 1916:303-309.
12. Levin-Allerhand, J.A., Sokol, K., and Smith, J.D. 2003. Safe and effective method for chronic 17beta-estradiol administration to mice. *Contemp Top Lab Anim Sci* 42:33-35.
13. Dobin, A., Davis, C.A., Schlesinger, F., Drenkow, J., Zaleski, C., Jha, S., Batut, P., Chaisson, M., and Gingeras, T.R. 2013. STAR: ultrafast universal RNA-seq aligner. *Bioinformatics* 29:15-21.
14. Yates, A.D., Achuthan, P., Akanni, W., Allen, J., Allen, J., Alvarez-Jarreta, J., Amode, M.R., Armean, I.M., Azov, A.G., Bennett, R., et al. 2020. Ensembl 2020. *Nucleic Acids Res* 48:D682-D688.
15. Ritchie, M.E., Phipson, B., Wu, D., Hu, Y., Law, C.W., Shi, W., and Smyth, G.K. 2015. limma powers differential expression analyses for RNA-sequencing and microarray studies. *Nucleic Acids Res* 43:e47.
16. Middelbos, I.S., Vester Boler, B.M., Qu, A., White, B.A., Swanson, K.S., and Fahey, G.C., Jr. 2010. Phylogenetic characterization of fecal microbial communities of dogs fed diets with or without supplemental dietary fiber using 454 pyrosequencing. *PLoS One* 5:e9768.
17. Kim, D., Hofstaedter, C.E., Zhao, C., Mattei, L., Tanes, C., Clarke, E., Lauder, A., Sherrill-Mix, S., Chehoud, C., Kelsen, J., et al. 2017. Optimizing methods and dodging pitfalls in microbiome research. *Microbiome* 5:52.
18. Bolyen, E., Rideout, J.R., Dillon, M.R., Bokulich, N.A., Abnet, C.C., Al-Ghalith, G.A., Alexander, H., Alm, E.J., Arumugam, M., Asnicar, F., et al. 2019. Reproducible, interactive, scalable and extensible microbiome data science using QIIME 2. *Nat Biotechnol* 37:852-857.
19. Callahan, B.J., McMurdie, P.J., Rosen, M.J., Han, A.W., Johnson, A.J., and Holmes, S.P. 2016. DADA2: High-resolution sample inference from Illumina amplicon data. *Nat Methods* 13:581-583.
20. McDonald, D., Price, M.N., Goodrich, J., Nawrocki, E.P., DeSantis, T.Z., Probst, A., Andersen, G.L., Knight, R., and Hugenholtz, P. 2012. An improved Greengenes taxonomy with explicit ranks for ecological and evolutionary analyses of bacteria and archaea. *ISME J* 6:610-618.
21. Bokulich, N.A., Kaehler, B.D., Rideout, J.R., Dillon, M., Bolyen, E., Knight, R., Huttley, G.A., and Gregory Caporaso, J. 2018. Optimizing taxonomic classification of marker-gene amplicon sequences with QIIME 2's q2-feature-classifier plugin. *Microbiome* 6:90.
22. Lozupone, C., and Knight, R. 2005. UniFrac: a new phylogenetic method for comparing microbial communities. *Appl Environ Microbiol* 71:8228-8235.

23. Lozupone, C.A., Hamady, M., Kelley, S.T., and Knight, R. 2007. Quantitative and qualitative beta diversity measures lead to different insights into factors that structure microbial communities. *Appl Environ Microbiol* 73:1576-1585.
24. Katoh, K., and Standley, D.M. 2013. MAFFT multiple sequence alignment software version 7: improvements in performance and usability. *Mol Biol Evol* 30:772-780.
25. Benjamini, Y., Drai, D., Elmer, G., Kafkafi, N., and Golani, I. 2001. Controlling the false discovery rate in behavior genetics research. *Behav Brain Res* 125:279-284.
26. Weljie, A.M., Newton, J., Mercier, P., Carlson, E., and Slupsky, C.M. 2006. Targeted profiling: quantitative analysis of 1H NMR metabolomics data. *Anal Chem* 78:4430-4442.
27. Rhoades, S.D., and Weljie, A.M. 2016. Comprehensive Optimization of LC-MS Metabolomics Methods Using Design of Experiments (COLMeD). *Metabolomics* 12.
28. Dieterle, F., Ross, A., Schlotterbeck, G., and Senn, H. 2006. Probabilistic quotient normalization as robust method to account for dilution of complex biological mixtures. Application in 1H NMR metabonomics. *Anal Chem* 78:4281-4290.